Chapter 4

Case studies on spatio-temporal analysis b-value before the occurrence of major events with respect to different regions

Chapter 4

Case studies on spatio-temporal analysis b-value before the occurrence of major events with respect to different regions

4.1 Introduction

The b-value is an important statistical parameter used in seismological studies. Numerous studies have been conducted over the globe to analyze the time varying character of the b-value preceding major events. Spatio-temporal anomalies in b-value, a measure of seismicity, often precede major earthquakes, offering crucial insights into seismic activity. These anomalies refer to deviations from the typical distribution of earthquake magnitudes and frequencies in a specific region over time. Observing shifts in b-values can signal changes in stress accumulation and release along fault lines, potentially indicating the buildup of seismic energy before a significant event. By analyzing these anomalies, seismologists can enhance earthquake forecasting and risk assessment, aiding in the implementation of proactive measures to mitigate the impact of future seismic events. In the previous chapter, the seismic zonation has been laid out. In synchrony with those demarcated zone along with additional active seismic zone, in this chapter, we have performed the 4-D (spatio-temporal and depth) analysis before the occurrence of four major recent events, including the Assam earthquake (28th April 2021, M_W 6.4), the Mizoram earthquake (26th November 2022, M_W 6.1), the Gaziantep, Türkiye Earthquake (6th February 2023, M_W 7.8), and the Nepal earthquake (9^{th} November 2022, M_W 6.3). Accordingly, the following sections will describe this spatio-temporal analysis pertinent to these significant events case by case basis.

4.2. The Assam earthquake (28^{th} April 2021, M_W 6.4)

4.2.1. Introduction

Northeast India experiences frequent earthquakes, with 18 major quakes in the past century. Significant events include the Shillong earthquake (1897, Mw 8.1) [1] and the Assam-Tibet earthquake (1950, Mw 8.4), causing substantial casualties and damage. The

Sarma, V., Bora, D. K. and Biswas, R. Spatio-temporal analysis of b-value prior to 28 April 2021 Assam Earthquake and implications thereof. Annals of Geophysics, 65(5): p. SE534, 2022.

region, particularly the Kopili fault area, is seismically active and lies between latitudes 24°-28°N and longitudes 90°-94°E. Seismic activity is influenced by the subduction of the Indian plate under the Eurasian plate. The FMD of earthquakes, defined by the GR equation (equation 1 as mentioned in chapter 2) [2] links earthquake occurrence to magnitude through coefficients 'a' and 'b', where 'b' reflects crustal characteristics and stress levels. Studies have shown correlations between 'b-value' and factors like Bouguer gravity, fractal dimension, and seismic moment in NE India [3], [4]. Research indicates b-values range from 0.5 to 1.5 [5], [6] and can act as earthquake precursors, as observed before major global quakes [7], [8]. This chapter focused on the Kopili fault, examining spatio-temporal b-value variations and dependencies on focal depth before the 2021 Assam earthquake (Mw 6.4). It includes an interplate model and correlational analysis incorporating macroscale heterogeneities.

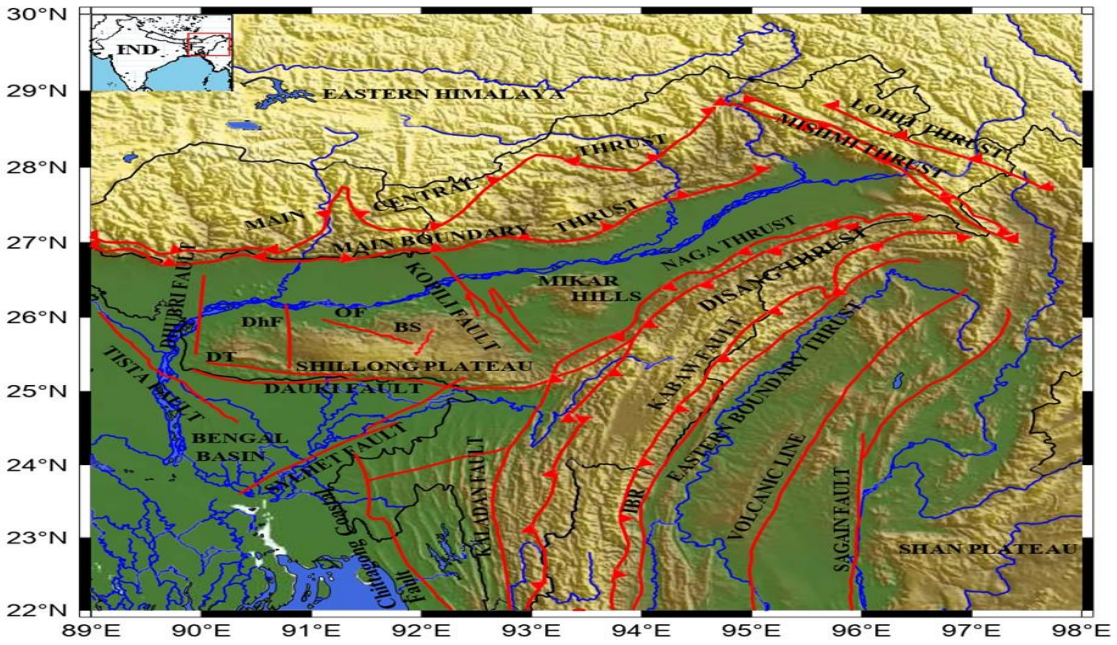

Figure 4.1: The topological plot of the NER of the Indian subcontinent shows various faults and thrusts. The prominent tectonic features in this region include; MCT, MBT, LH: Lohit thrust, MT: Mishmi thrust, KF, SF: Sagaing fault, DF, DT: Dapsi fault, DhF: Dudhoni fault, Dhubri fault, Tista fault, Kaladan Fault, CCF: Chittagong Coastal Fault, OF, BS: Barapani shear zone, NT, Kopili fault. The major thrusts located are shown by the teeth lines. Inset map showing the highlighting study region.

4.2.2. Tectonic setup

In Northeast India, as depicted in Figure 4.1, seismic activity is prominently influenced by the subduction of the Indian plate beneath the Eurasian plate [9]. The study area, illustrated in Figure 4.2, encompasses three major tectonic zones: the eastern Himalayan zone, the Assam valley region, and the Shillong plateau region, delimited by latitude 24°-28°N and longitude 90°-94°E. The Mikir hill plateau hosts the active Bomdila and Kopili faults. The Kopili Fault, spanning 300 km in a NW-SE direction and 50 km in width, extends from western Manipur to the Bhutan-Arunachal Pradesh-Assam trijunction. The 2009 Bhutan earthquake, originating from the KF, highlights its active seismicity and expansion towards the MCT in the Bhutan Himalaya. Located at the junction of the MBT and MCT, the Kopili Fault experiences heightened seismic activity, as evidenced by the August 19 and September 21, 2009 earthquakes. These events are characterized by shallow-focus, right-lateral strike-slip faults, indicative of ongoing compression from the Indo-Burmese arc and the Himalayan arc. The seismogenic zone of the Kopili Fault extends down to a depth of 47 ± 2 km [10], increasing in depth from northern Burma towards the MCT. Figure 4.2 also identifies the epicenter of the April 28, 2021 earthquake (Mw 6.4).

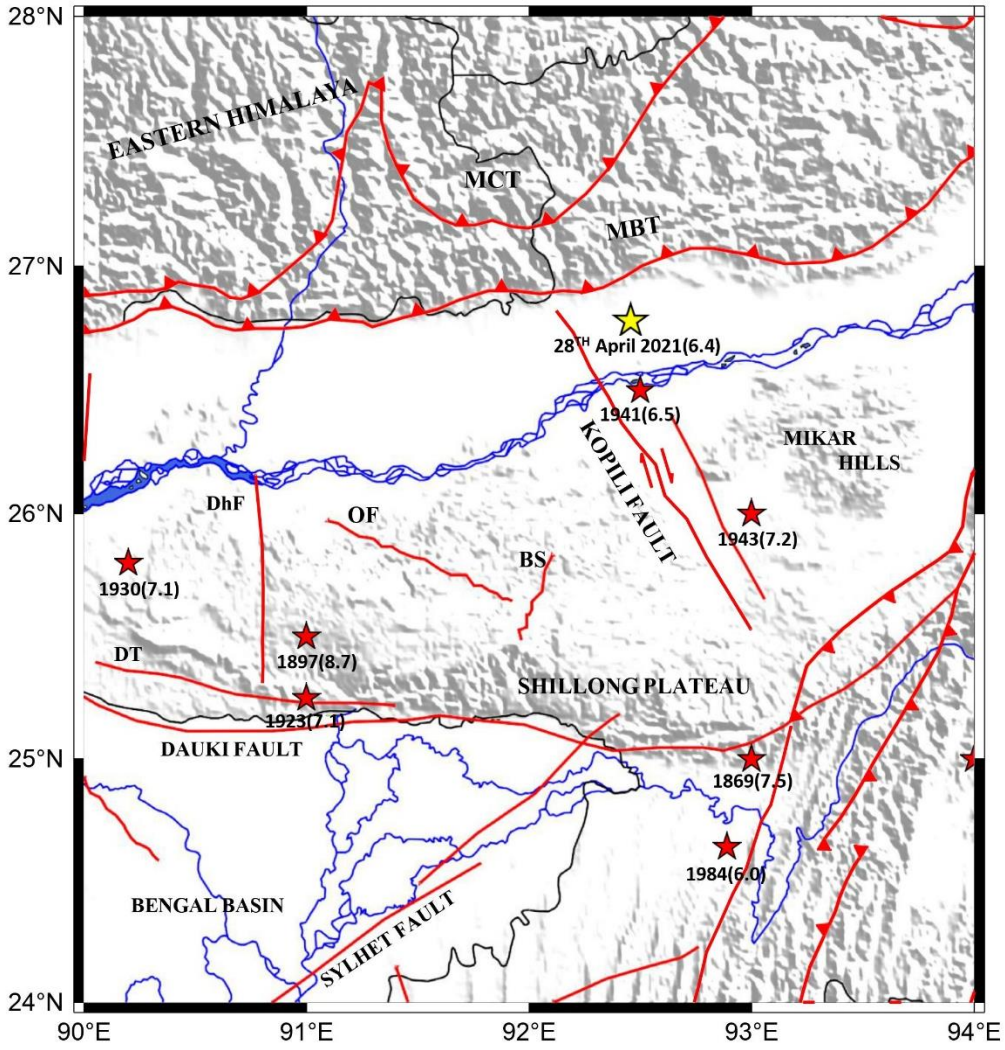

Figure 4.2: The tectonic plot of the study region. the major earthquake events that happened in this region are shown by red stars. The epicentral location 28th April 2021 earthquake is shown by the yellow star. MBT: Main boundary thrust, MCT, OF, KF, NT, DF, SF, DT, DhF, BS, Kopili fault. The thrust lines are shown by the teeth lines.

4.2.3. Data analysis

We compiled a catalog of 1398 earthquakes occurring between 1950 and 2021, with magnitudes ranging from 2 to 8, sourced from the International Seismological Center (ISC) and the United States Geological Survey (USGS). Using the [11] (as mentioned in Table 2.2 of chapter 2) model, we distinguished mainshocks from aftershocks and standardized magnitudes to Mw based on [12] and [13] (as mentioned in Table 2.1 of chapter 2). The Mc was determined using the MAXC method with bootstrapping, yielding Mc=3.9 (as shown in Figure 4.3) after applying a correction factor.

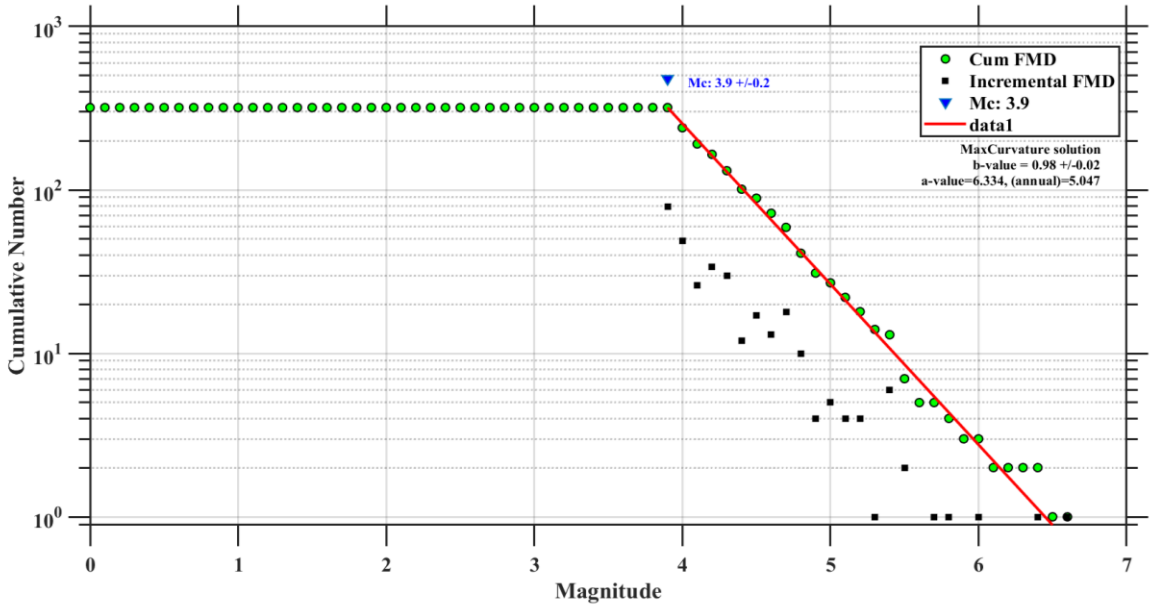

Figure 4.3: FMD of earthquakes from 2000 to 2021. The straight line is the best fit. The M_C value and the average b-value for the complete study region.

A notable decrease in M_C post-1993 (as shown in Figure 4.4) was attributed to network improvements and increased seismic activity (as shown in Figure 4.5).

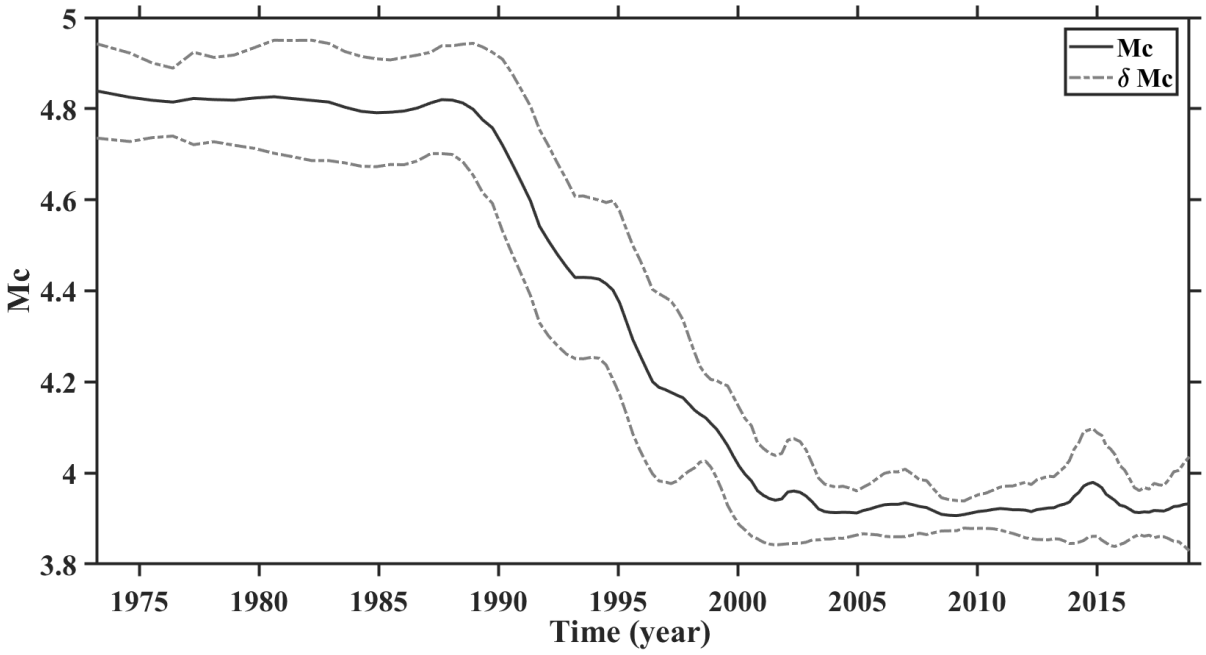

Figure 4.4: Plot of the Mc variation with time. Standard deviations are shown by dashed lines.

We analyzed 750 events with $M_W \geq M_C$ to compute the b-value, confirming data linearity using the GR power fit law with the MLE method.

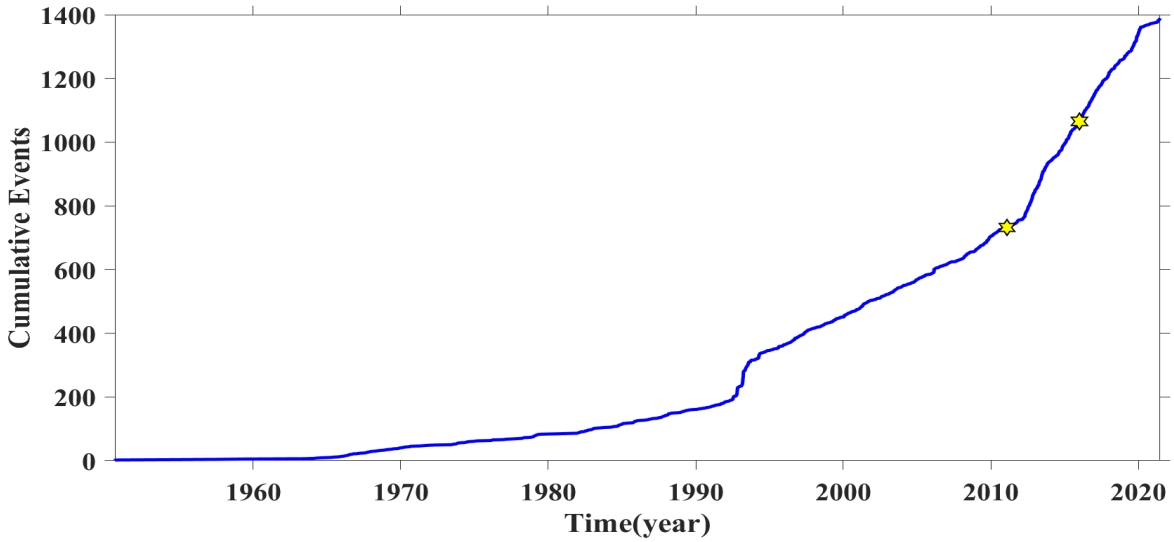

Figure 4.5: plot of the Cumulative number of earthquake events as a function of time of the region.

Figure 4.6 depict the epicentral distribution of earthquakes from 1950 to 2021 with magnitude $M_W \geq 3.9$ used for the b-value analysis.

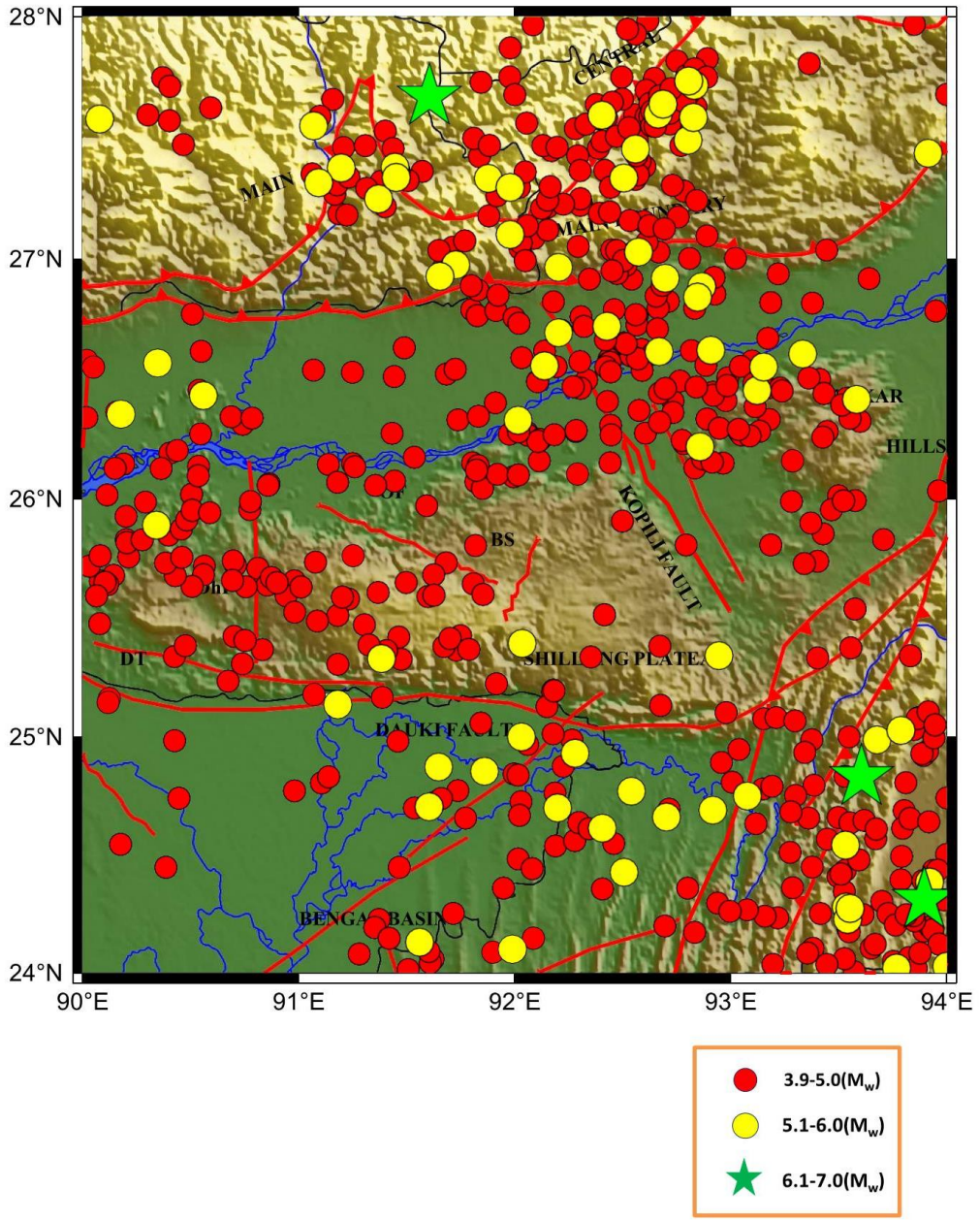

Figure 4.6: The epicentral location of all the earthquake events observed in this region (1950-2021) having Mw ≥ Mc is shown in the plot.

4.2.4. b-value estimation

The present chapter is based on the MLE suggested by [14] and [15]. Furthermore, the SD of the b value is estimated using the relationship proposed by [16]. The average b-value derived from this method is b=0.98± 0.2, as illustrated in Figure 4.3.

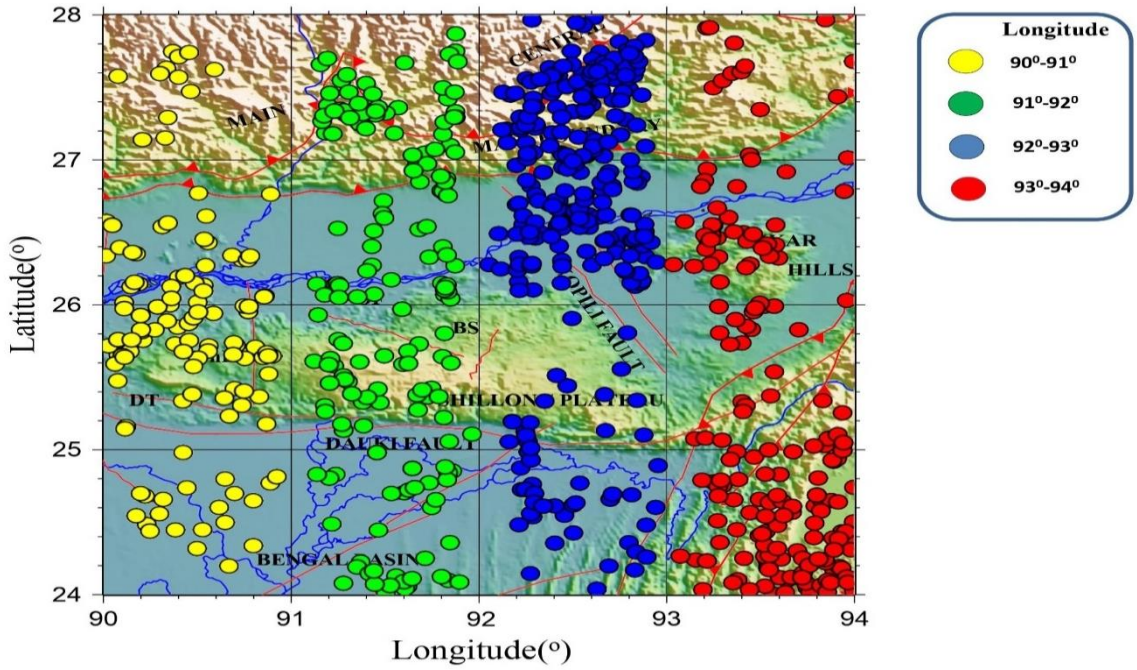

Figure 4.7: The epicentral location of all the earthquake events recorded in the study region from 1950 to 2021. The longitude-wise distribution of these earthquakes is shown by yellow, green, blue, and red marks.

For the spatial variation of the b-value, the entire study region is subdivided into 16 equisized grids of $1^{o}\times1^{o}$ dimensions. The moving window of 0.5° × 0.5° has been chosen to retain the natural grid to grid continuity of data points. Several available reports ([17], [18], [19], [20], [8]) opined that sufficient data should be present for reliable and better analysis of b-value; otherwise, less quantity of seismic data may result in undesired and incorrect results. As a result, accuracy and coverage suffer. Thus, adequate seismic data is required for a better and high-quality outcome. Table 4.1 depicts the b-value for each grid and the events that are used for the calculation are shown in Figure 4.7. The b-value variation as a function of time is shown in Figure 4.8. The phenomena of significant fall in b-value prior to any main event can be established from the Figure 4.8.

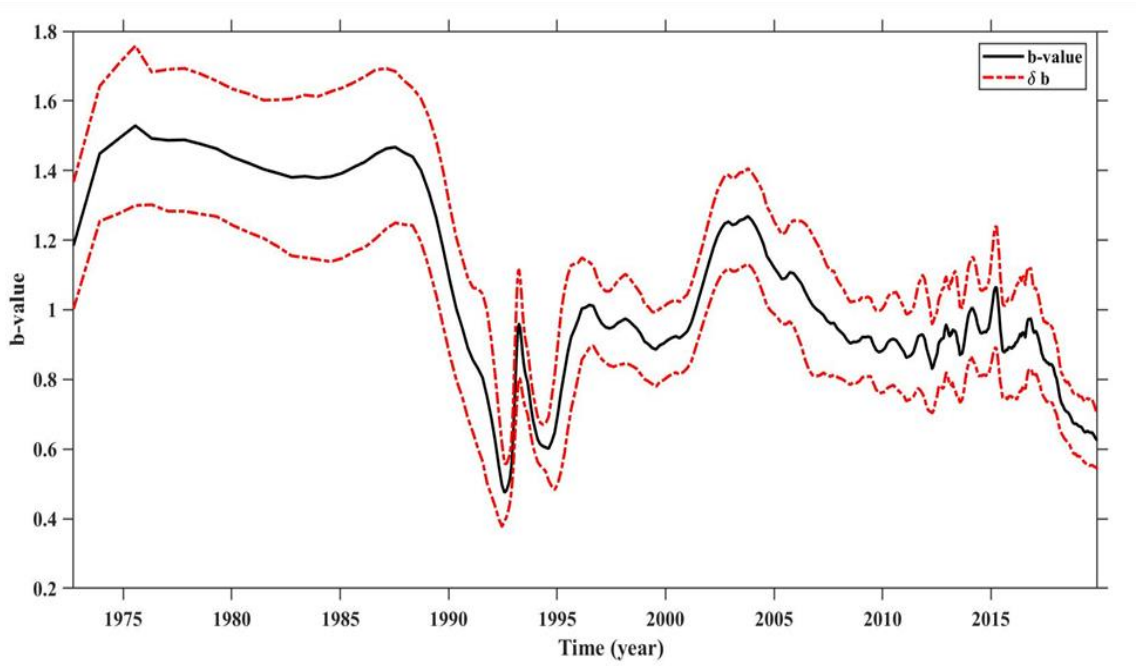

Figure 4.8: The time series projects the variation in b-value for the study region. A significant fall in b-value can be traced. The SD is shown by the dashed line.

Table 4.1: Spatial variation of b-value for study region

Longitude(°E)	Latitude(°N)	Nmin	b-value
90-91	24-25	14	0.95
90-91	25-26	63	1.25
90-91	26-27	53	0.94
90-91	27-28	23	0.76
91-92	24-25	49	0.80
91-92	25-26	58	0.84
91-92	26-27	61	0.88
91-92	27-28	60	0.71
92-93	24-25	52	0.68
92-93	25-26	31	0.73
92-93	26-27	139	0.76
92-93	27-28	155	0.72
93-94	24-25	129	0.76
93-94	25-26	49	0.66
93-94	26-27	65	0.83
93-94	27-28	33	0.88

The relationship between the b-value and focal depth is also examined. The next section presents a more in-depth analysis of these results. The declustring, earthquake completeness of the earthquake catalog, and spatio-temporal, depth-weighted analysis of the b-value are carried out using the Zmap tool ([21]).

4.2.5. Results and discussions

Recent studies ([22], [23], [24], [25], [26]) inferred that the b-value can vary with several factors including depth, stress accumulation, plate tectonics, and faulting style mechanism. Due to the subduction of the Indian plate under the Eurasian plate, this region remains under high stress [27]. Figure 4.9 appraises the variation of b-values with focal depths of the seismic events. The 8 slabs with each slab having a focal depth of 10 km are projected by virtually dividing the area under investigation. The b-value is plotted against each slab as projected in Figure 4.9. The lowest b-value is associated with the upper crust. Similar implications were made by [24] for the entire NE India and quoted that a low b-value is observed at a depth range of 25 km to 36 km. The lower b-value detected at a deeper depth range for the southwest part of the study area may be allied with the rising protuberant of the lithosphere in this region. The low b-value in the upper crust implies crustal homogeneity. We encounter a low value of 0.66-0.71 confined to the upper crust. The obtained result is plausible with the results that the accumulation of crustal stress in the upper crust is more associated with the in-depth region.

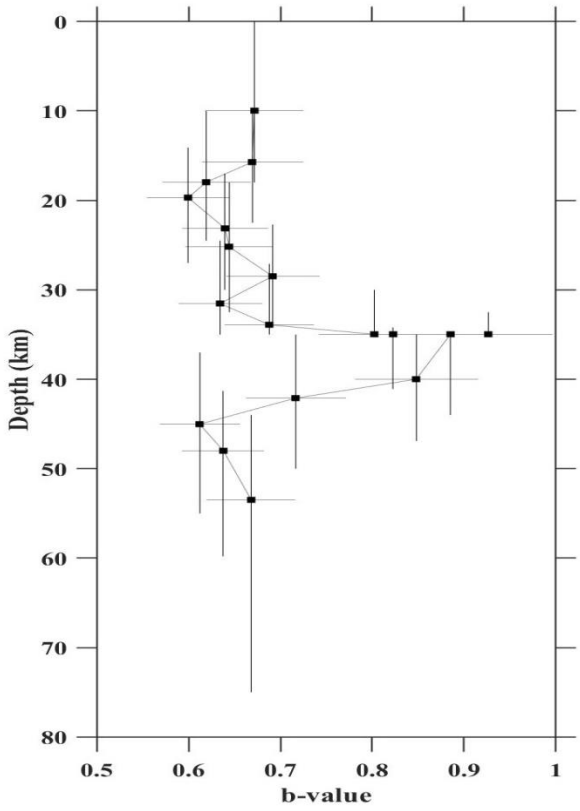

Figure 4.9: Graph showing the variation in b-value concerning depth for the study region.

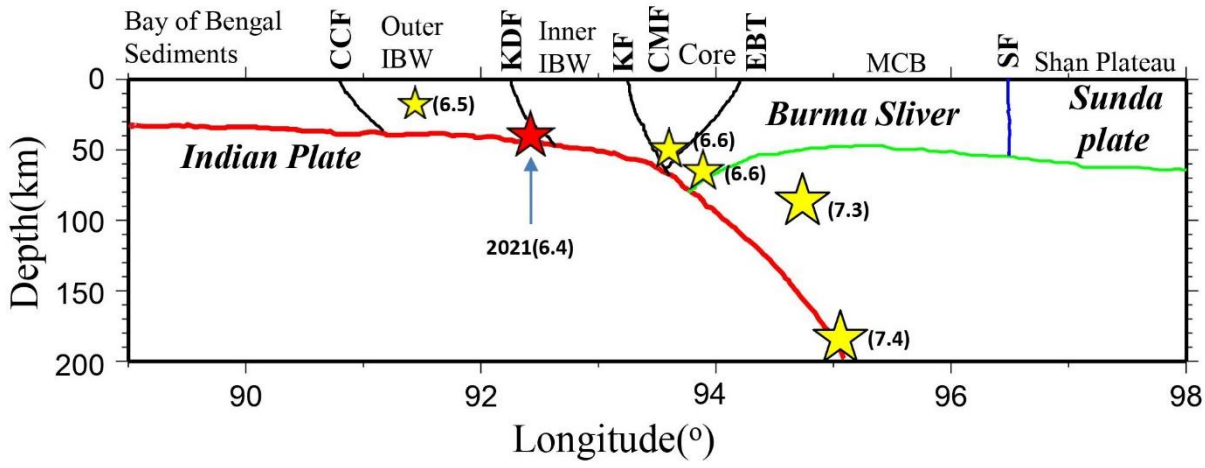

Figure 4.10: the seismotectonic model shows the epicentral location of all the events with magnitude Mw ≥6.5 observed in this region. The epicentral location of the recent 28th April 2021(6.4) earthquake is shown by a red star.

The interplate model helps us to approximate the location of the 28th of April 2021 (Mw 6.4) earthquake (Figure 4.10). It is an interplate earthquake with a reported depth of ~34 km [26]. Mostly interplate earthquakes are observed in this region (Figure 4.10). It is

stated that crustal homogeneity and high seismic moment are implicated by lower b-values. Notably, the 2021 event occurred at a depth of 34 km, hinting at the accumulation of stress in the upper crust of the subduction region. As per [27], subcrustal earthquakes showed depth ranges from 20 to 50 km. Meanwhile, in another study by [28] higher b-values were obtained at intermediate depths of 80-100 km beneath Guatemala El-Salvadore as well as for deeper depths of 130-170 km about Nicaragua. A recent study by [4] reported that the b-value is less than unity down to 50-55 km depth, and there is a sharp rise in b-value near 60 km depth in IBR. In similitude to these observations, the current study attains higher b-values in intermediate depth (40-45 km) as well as for deeper depth regions. The study conducted by [29] in New Zealand and Alaska respectively report high b-value anomalies on top of the subducting slabs at depths within 100-150 km depth range. Further, it is observed that the number of events with focal depths greater than 70 km shows a declining trend. Lower tectonic stress at deeper depth with the accompaniment of a high b-value could be one of the prominent causes of this observation. The depth histogram as shown in the Figure 4.11 reveals that there is a significant rise in earthquake events for the depth range 30 km to 50 km and the maximum peak is observed at the focal depth of 35 km and the 28th of April 2021 (Mw 6.4) is also reported at the focal depth of 34 km. The same implications are reported by [23] that earthquakes events in the study region occurred at the focal depth of 30 km to 50 km. Likewise, Figure 4.12 reveals that the number of earthquakes having magnitude $M_W\sim$ (4-5) is more and only a few events having magnitude $M_W \geq 5$ are observed in this region. The spatial variation of the b-value for the study region is shown in Figure 4.13. The result shows that the b-value varies from 0.66 ± 0.09 to 1.24 ± 0.11 for the study region. [23] inferred that the b-value for northeast India varies from 0.23 to 1.78. Similar implications were made by [4] for the Indo-Burma region in which the b-value varies from 0.7 to 1.5.

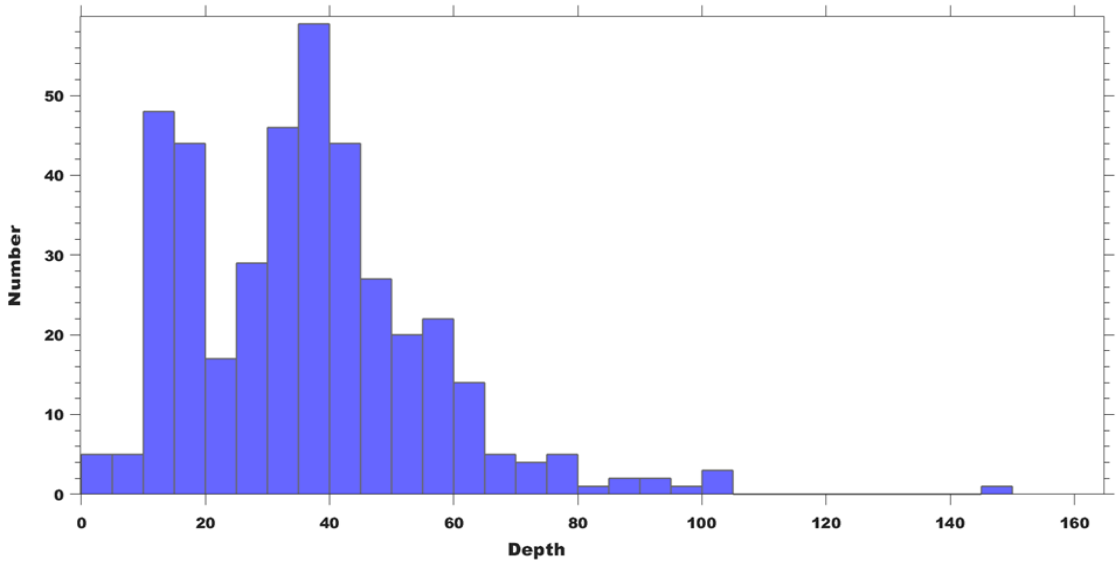

Figure 4.11: Histogram showing depth-wise variation corresponding to chosen 750 events (Mw ≥ 3.9). The intense seismicity is reported at the focal depth of 30km to 50km.

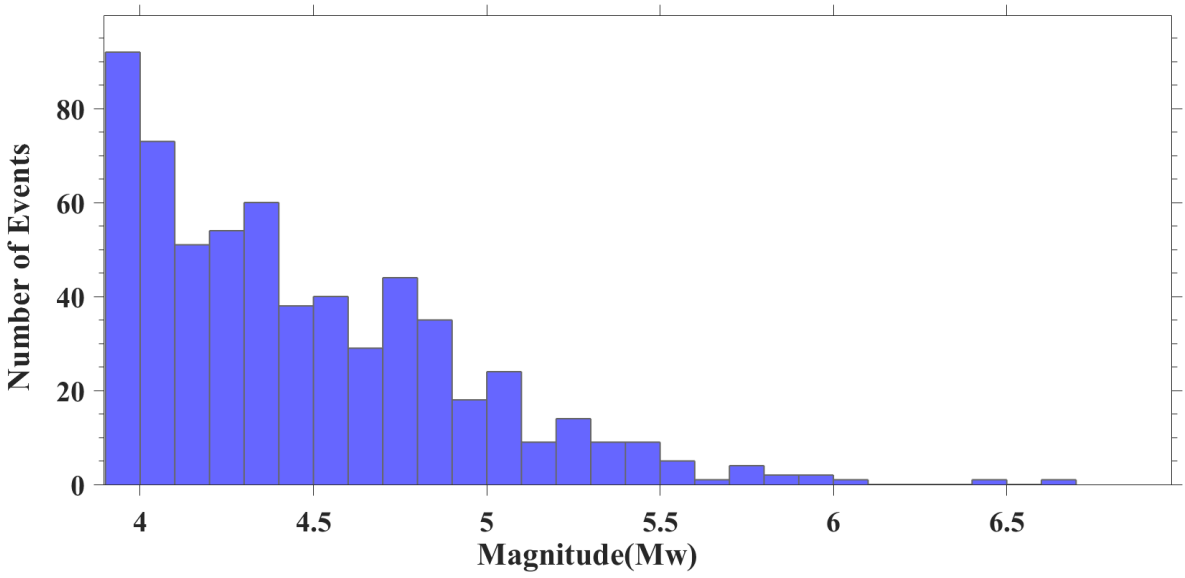

Figure 4.12: Histogram shows the number of earthquakes versus Magnitude for the selected 750 events (M_W≥3.9). Mostly small magnitude earthquakes with some large magnitude earthquakes are observed in this region.

Thus, the observations made from our study show a plausible relationship with already existing results. A recent study [8] reported an intermediate b-value before the Manipur earthquake (2016).In the present study, low b-value variation is also observed in the regions between 25-26°N and 93-94°E. These have been suggested to be due to large variations in tectonic stress owing to local variations in the plate tectonic driving forces.

[30] successfully explained the seismicity and the subduction process by testing the correlation between coupling and other physical features of subduction zones. In contrast, a significant low variation of b-values is observed (Table 4.1) around the epicenter of the 28th April 2021 (Mw 6.4)Assam earthquake (Lat ~26.781°N, Long ~92.457°E), where the b-value concentrates around 0.76. The implications made after a global scale study of b-value for the large region show b-value near to unity for any seismically active region but a recent study [23] shows the variation in b-value up to 1.78. Our results show good agreement with the already existing studies for the northeast Indian region (eg. [23], [4]). Certain areas of the study area embody higher stress accumulation relatively. This may be treated as an implication of future impending larger ruptures related to these locations. Since the Kopili fault and its neighboring areas are active regions, the current work will prove to be useful for earthquake prediction and seismic hazard assessment.

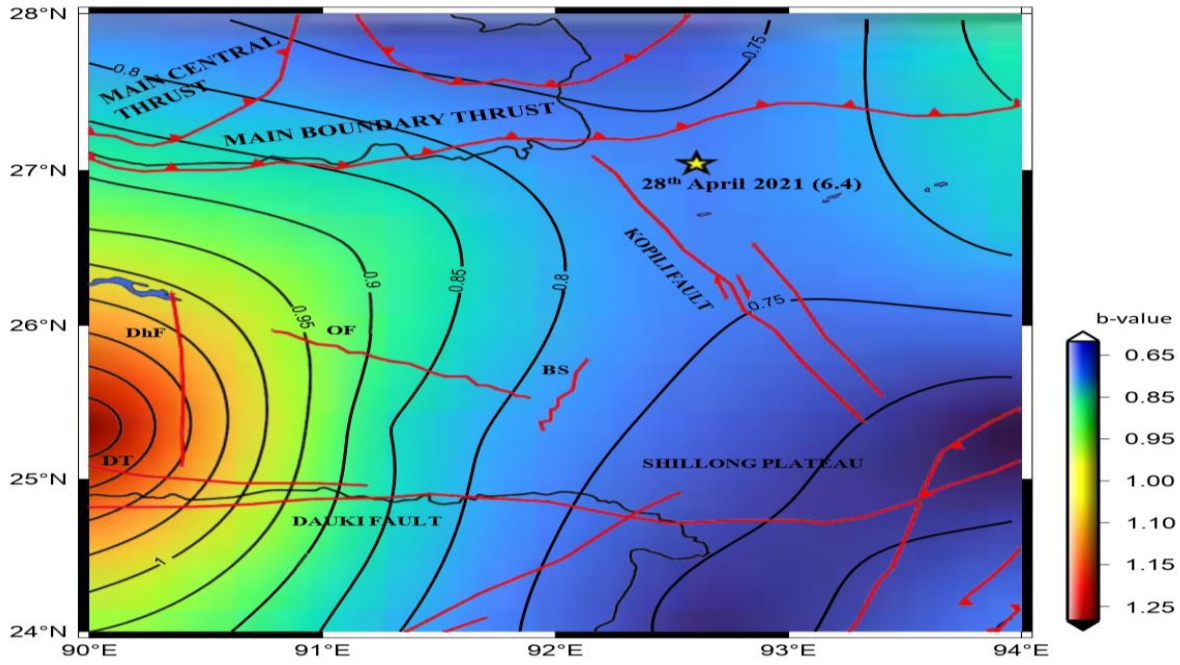

Figure 4.13: b-value contour map for the study region. The epicentral location of the 24th April 2021 earthquake is shown by the yellow star.

4.3. The Mizoram earthquake (26th November 2022, M_W 6.1)

4.3.1. Introduction

The northeastern region of India, designated as zone V [31] for seismic activity, is characterized by its diverse geological features, including the eastern Himalayas, Shillong plateau, Indo-Burma region, and Brahmaputra plains (as shown in Figure 4.14). The constant subduction of the Indian plate beneath the Burmese plates results in frequent seismic events, making it a hotspot for major earthquakes. Recognizing the significance of the b-value, this chapter investigates the b-value variation in the region as a potential earthquake precursor, focusing on events preceding the November 26, 2021 Mizoram earthquake (M_W 6.1). This meticulous investigation fills gaps left by conventional techniques, highlighting the importance of statistical tools in seismic research.

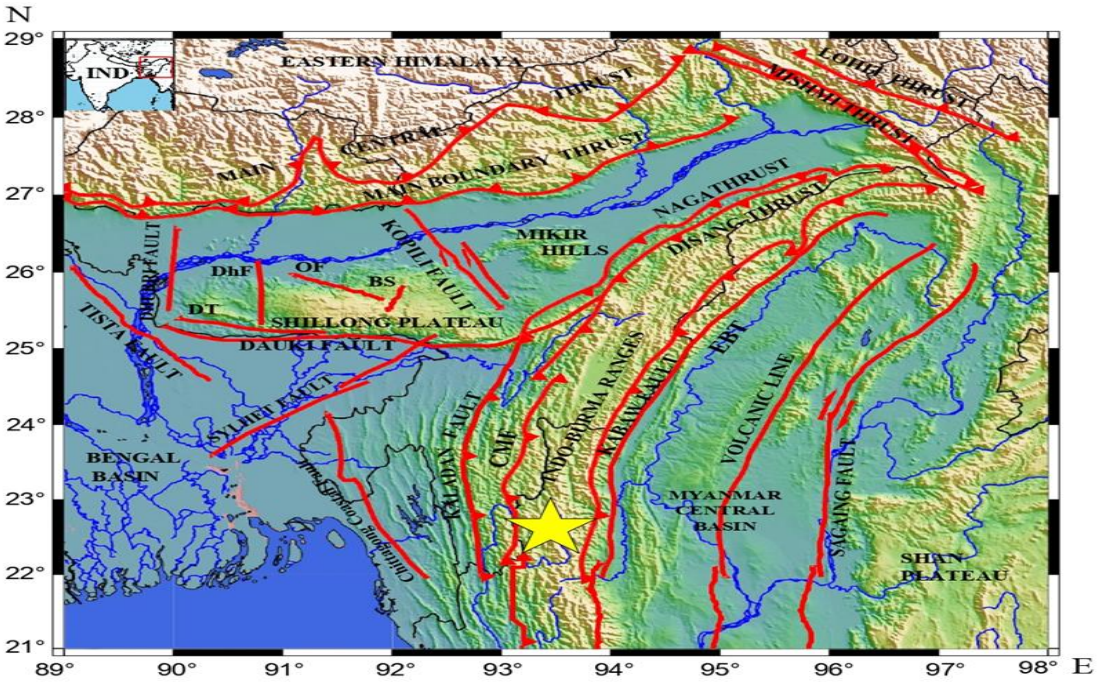

Figure 4.14. The tectonic plot of entire NE India. The epicentral location of the 26th November Mizoram earthquake (Mw~6.1) is shown by a yellow star. An inset map of India marking the study region is shown at the top left corner.

4.3.2. Tectonic setup

The tectonic map of NE India (Figure 4.14) shows the N-S trending IBR, a region prone to major earthquakes due to the subduction of the Indian plate under the Burmese plate, which began in the Cenozoic era. The IBR extends from the Eastern Himalayan Syntaxis (EHS) in the north to the Andaman spreading zone in the south. The EHS serves as a transition between the MCT and MBT and connects to the IBR. The KF forms a boundary between the Myanmar Central Basin (MCB) and IBR, while the SF separates the MCB from the Shan plateau and connects to the Andaman Spreading Ridge (ASR) [32]. The NT separates the eastern Assam valley from the IBR, and the active Churachandpur Mao Fault (CMF) runs through the IBR [33].

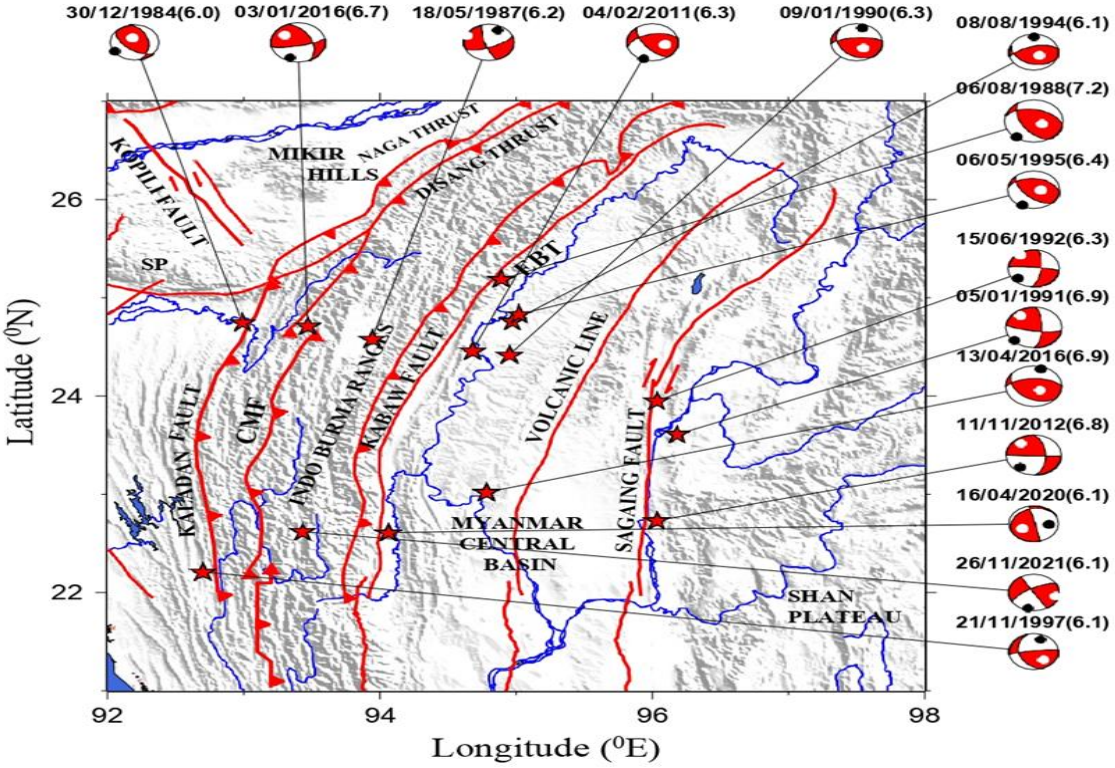

Figure 4.15: The focal mechanism solutions and epicentral location of the earthquakes with magnitude $M_W \geq 6$ are presented in the figure.

Figure 4.15 shows seismogenic characteristics and epicenters of earthquakes ($M_W \geq 6.0$) in the region since 1976, with most exhibiting a thrust mechanism indicating under thrusting. Five of the eight large earthquakes have epicenters along the EBT, further illustrating this under thrusting. The GCMT provides focal mechanisms for these significant earthquakes.

4.3.3. Data Analysis

The b-value, a factor indicating earthquake size distribution, was analyzed using an earthquake catalog spanning from 1964 to 2021 for the region between 22°–27° N latitude and 92°–97° E longitude. This catalog, sourced from ISC and USGS, includes 3,154 events with magnitudes (Mw) of 3.5 or higher. To ensure accuracy, aftershocks and foreshocks were separated, and duplicate entries were removed using the [11] (as mentioned in Table 2.2 of chapter 2) declustering method. The cumulative increase in the number of events is illustrated in Figure 4.16.

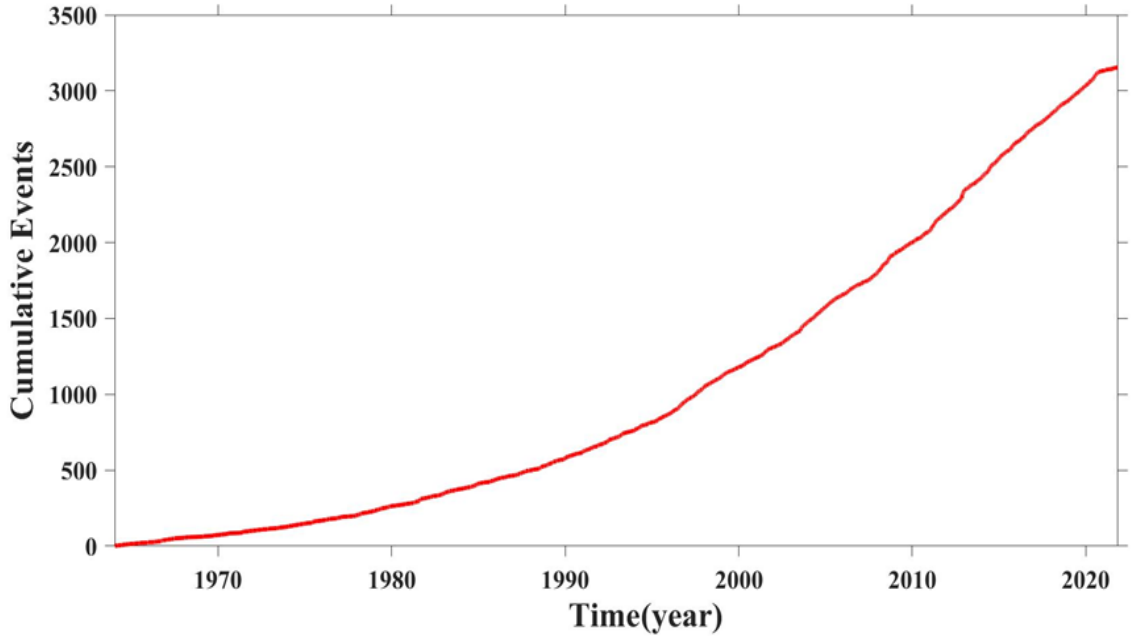

Figure 4.16. The plot depicts the cumulative number of earthquakes in the area as a function of time.

Magnitudes were converted to Mw using the conversion formulas proposed by [12] and [13] (as mentioned in Table 2.1 of chapter 2) to maintain consistency. The M_C was calculated using the MAXC method as described by [34] and [35], with additional support from bootstrapping techniques [36]. Figure 4.17 illustrates the temporal variation in the M_C for the earthquake catalog.

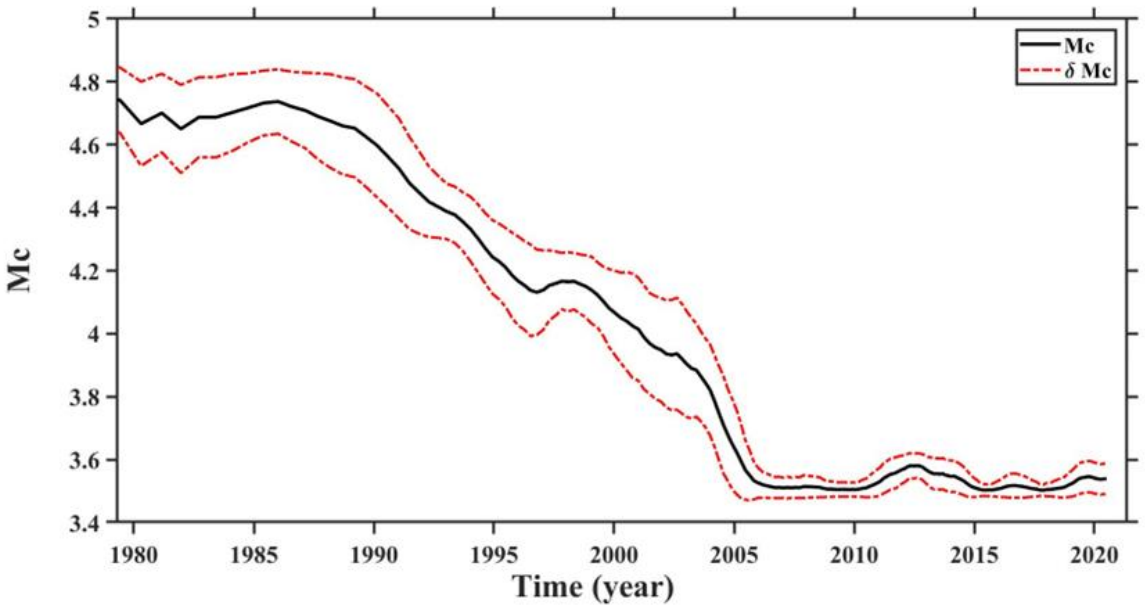

Figure 4.17: Plot of the M_C. The SD in value is projected by the dashed line.

As previously discussed, the variations observed in the M_C value can be attributed to the upgrades and changes in the seismic network within the study region. Notably, the average M_C value for the study area is 3.9, as depicted in Figure 4.18.

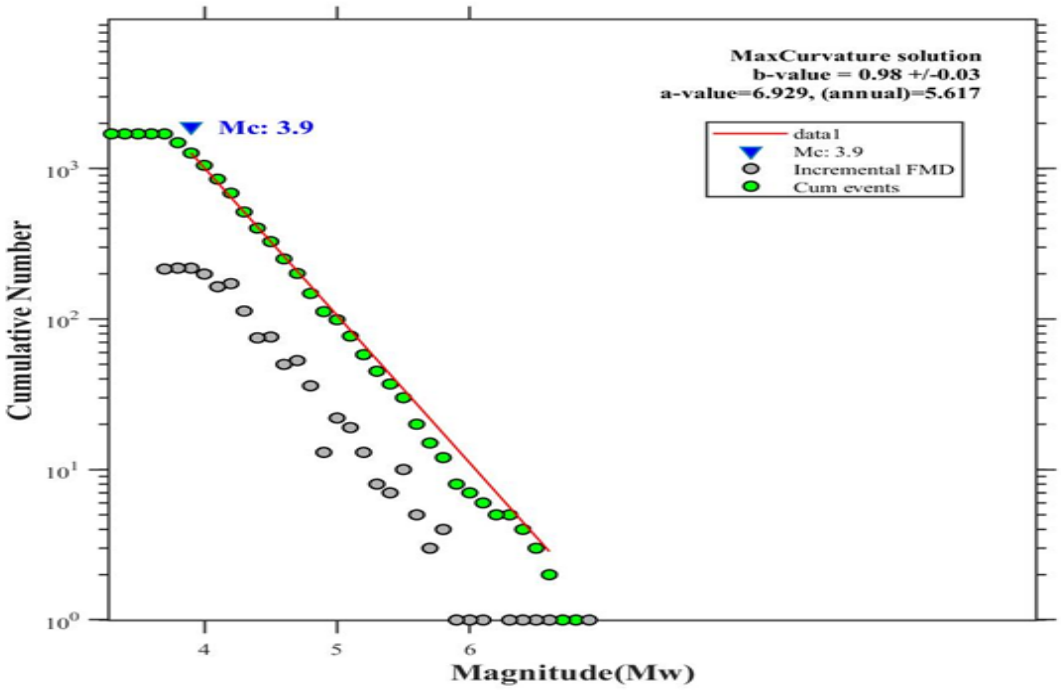

Figure 4.18: Shows the FMD plot for the database, including the M_C, and the mean b-value for the study region.

For precise analysis, 767 well-located events (as shown in Figure 4.19) from ISC-EHB and GCMT databases with Mw≥3.9 were used to perform spatial-temporal and depth-wise b-value variation analysis.

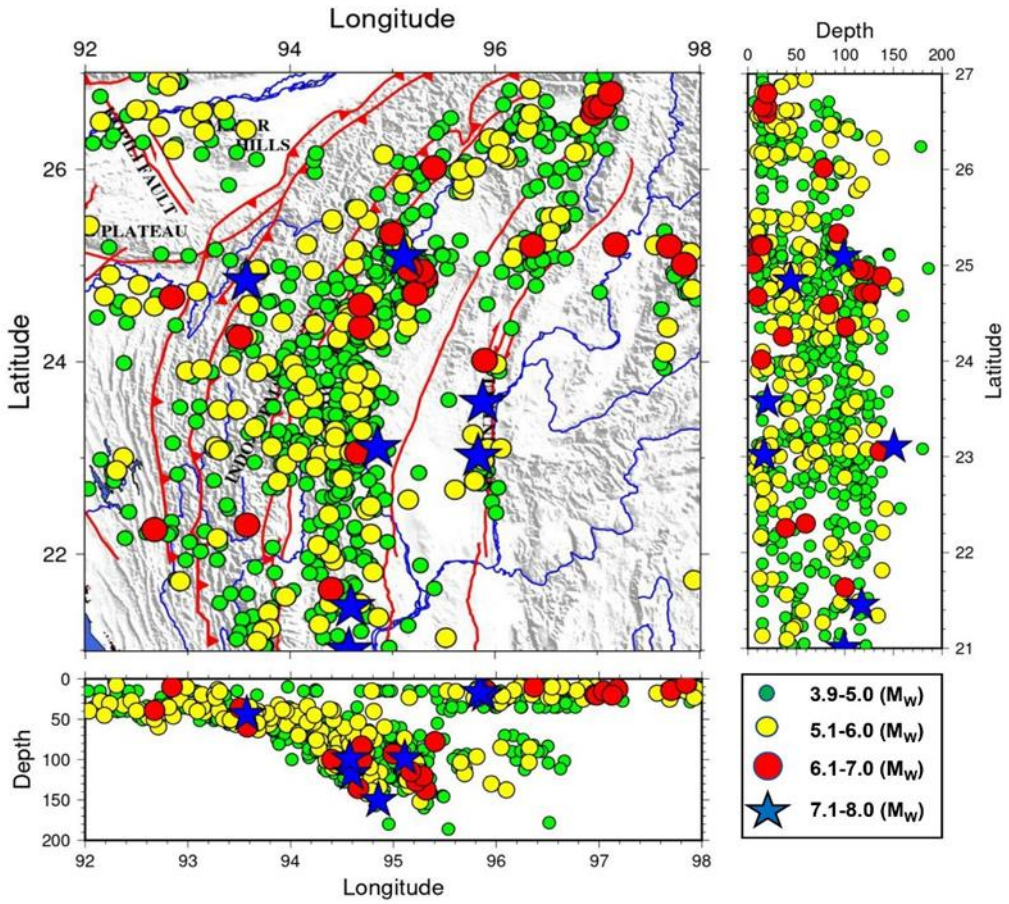

Figure 4.19: The plot depicts the epicentral location of all the (767) events with $M_W \geq M_C$.

4.3.4. b-value calculation

The Aki-Utsu MLE [14], [15] is used to approximate the average b-value and the SD in b-value is estimated using [16] method. The average b-value derived from this method is b=0.98 ± 0.3, as illustrated in Figure 4.18. The Zmap tool [21] is used for spatio-temporal and depth-wise variance analysis. Temporal and depth variations in the b-value help assess stress accumulation and predict major events. The non-parametric K-S test determines the significance of these variances.

4.3.5. Results and Discussions

The geospatial variation of the FMD factor of earthquakes (b-value) for the study region is detailed in Table 4.2 and visually represented in Figure 4.20. To analyze this spatial variation, the entire research area is alienated into equal-sized grids of 2° × 2°, with a 1° × 1° movable window used to maintain consistency between data points across grids. A total of 767 earthquake events, sourced from the ISC-EHB earthquake catalog, were grouped based on their geographical location within these grids (Table 4.2). The MLE was then applied to estimate the b-value for each grid. The b-value for the study area ranges from 0.84 to 1.51, as shown in Figure 4.20.

Table 4.2: The geospatial distribution of the b-value is listed below

Longitude	Latitude	Freq	b-value	δb
92-94	21-23	62	1.18	0.19
92-94	23-25	74	0.88	0.12
92-94	25-27	42	1.20	0.20
94-96	21-23	127	0.92	0.08
94-96	23-25	241	0.91	0.07
94-96	25-27	83	0.84	0.02
96-98	21-23	3	0	0
96-98	23-25	23	1.51	0.25
96-98	25-27	112	0.87	0.05

Grids with inadequate data points are depicted in Figure 4.20 by the grey colour grid.

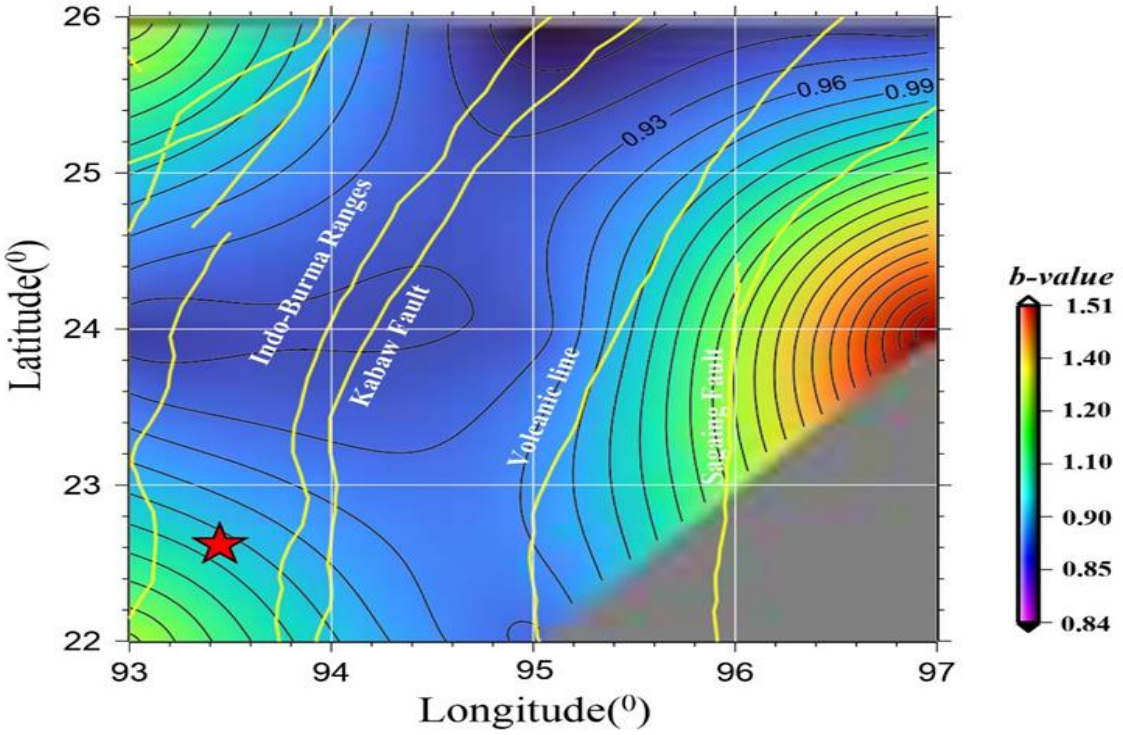

Figure 4.20: The geospatial distribution in b-value for the study region before the Mizoram earthquake (26th November 2021, M_w 6.1) is shown in the figure. The red star shows the epicentral location of a recent major earthquake.

A non-parametric K–S test was employed to assess the significance of the geographical distribution of b-values. The results of the K-S test calculations are presented in Table 4.3, where the Maximum D-value (Dmax) exceeded the critical D-value at significance levels of p = 0.05 and p = 0.02 with n=8. Consequently, the null hypothesis suggesting no substantial difference in b-value geographic distribution was rejected. Figure 4.21 displays a plot of cumulative probability against b-values following the K–S analysis, where Dmax represents the maximum modulus of difference between the empirical cumulative distribution function (ECDF) and the standard cumulative distribution function (SCDF). [37] utilized a similar statistical approach to assess temporal and spatial b-value distribution relevance prior to the Sichuan, China earthquake (2021, M_S 6.0).

Table 4.3. The parameters used in the K-S significance test for the geospatial distribution of the b-value are listed in the table below.

b-value	Freq	Cum Freq	ECDF	Z-value	SCDF	D-value
0.84	1	1	0.125	-0.84	0.201	0.076
0.87	1	2	0.25	-0.714	0.238	0.013
0.88	1	3	0.375	-0.671	0.252	0.124
0.91	1	4	0.5	-0.545	0.294	0.207
0.92	1	5	0.625	-0.502	0.308	0.318
1.18	1	6	0.75	0.597	0.725	0.026
1.2	1	7	0.875	0.682	0.753	0.123
1.51	1	8	1	1.992	0.977	0.024

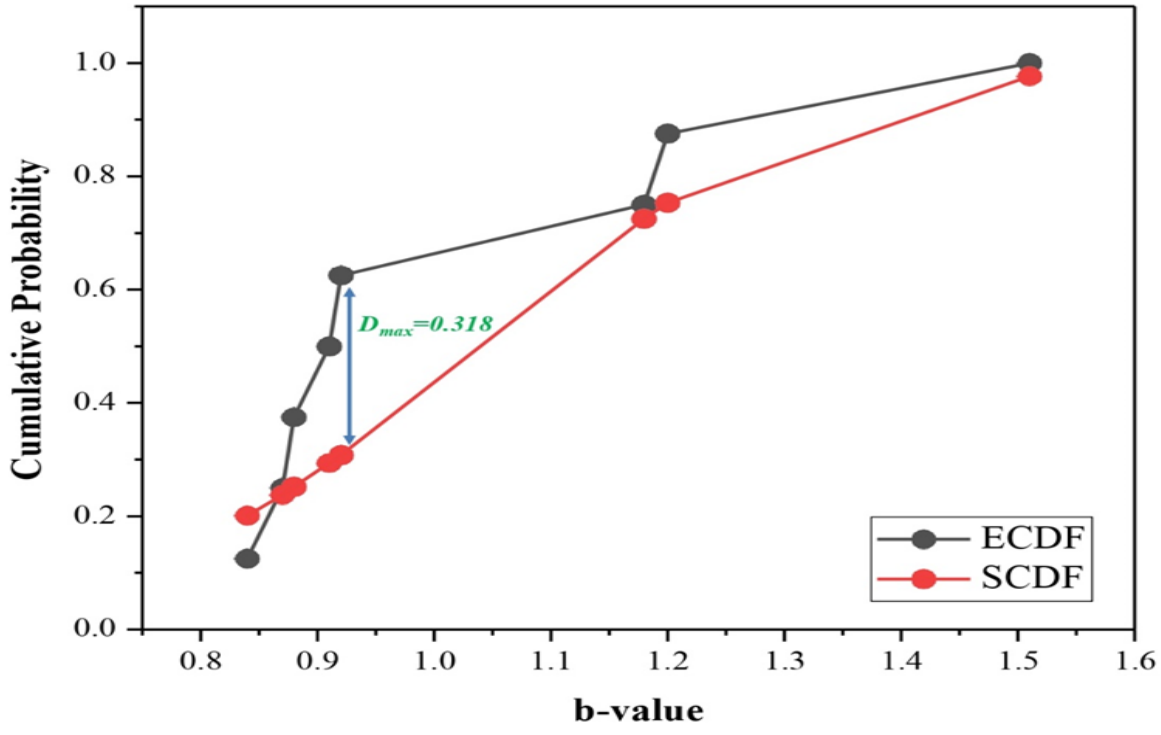

Figure 4.21: The Cumulative probability vs b-value using the K-S test to testify the significance of the geographical distribution of the b-value is shown in the plot.

[23] provided an extensive analysis of b-value variations across Northeast India, revealing a broad range from 0.23 to 1.78. Similarly, studies by [4] and [38] highlighted spatial

discrepancies in b-values within the IBR, spanning from 0.70 to 1.50. In our investigation, we identified a low b-value of 0.84 within the grid spanning 25^0-27^0N and 94^0-96^0E, contrasting with a peak b-value of 1.51 in the grid from 23^0-25^0N and 96^0-98^0E. Notably, a significant reduction in b-value was observed along the KF, originating from the historic 1762 Arakan earthquake. The southeast-trending KF, which run parallel to the IBR near Mizoram, along with the nearby SF, exert notable influence on the tectonic characteristics of surrounding faults, contributing to the occurrence of numerous major earthquakes in this region [39]. [40] documented substantial declines in b-value preceding major earthquakes, including the Sumatra events of 2002 and 2004. Figure 4.19 underscores that the majority of earthquake epicenters are situated in regions characterized by low b-values (Figure 4.20), particularly along the IBR near the Kabaw and SF, likely influenced by the relative motion between India and the Sunda plate ([39], [41]). The epicenter of the November 26, 2021 Mizoram earthquake was located within an intermediate b-value grid (Figure 4.21), consistent with findings from the January 3, 2016 Manipur earthquake observed by [8]. [42] studying various seismic regions of Iran, noted significant declines in b-values prior to major earthquakes, ranging from 0.58 to 0.91. Similar observations were made by [34] in the San Andreas zone, where decreases in b-values preceded significant seismic events in active regions of the western US and Japan.

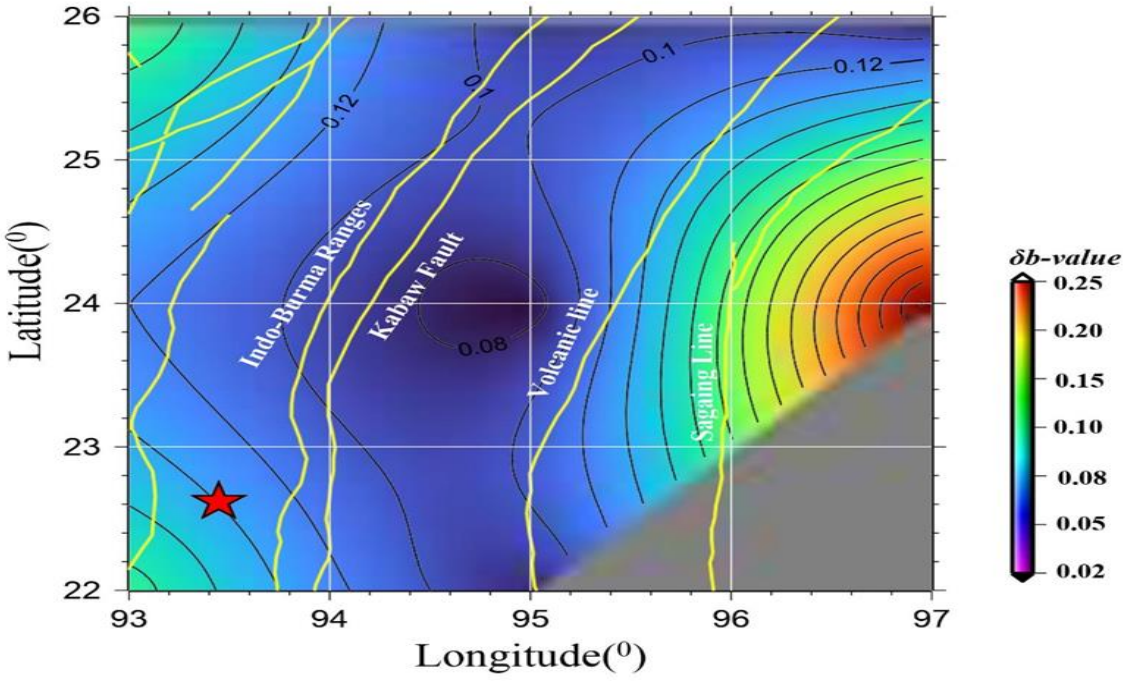

Figure 4.22: The plot illustrates the spatial distribution of SD reported in the b-value estimation.

The SD of the b-value for the study region which varies from 0.02 to 0.25 (Figure 4.22).

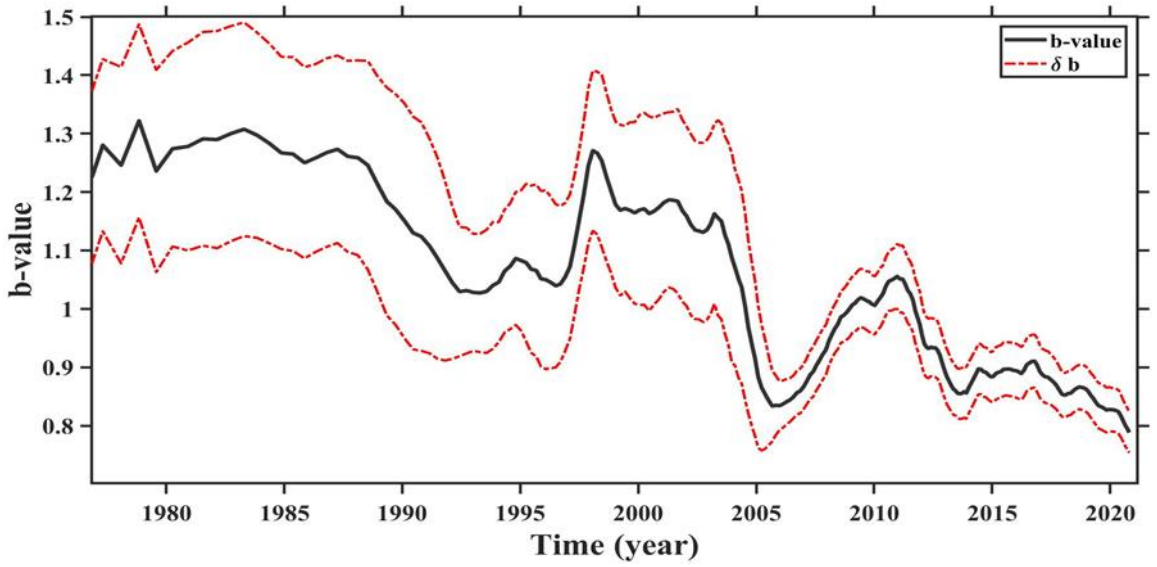

Figure 4.23: The plot illustrates the temporal b-value and the SD of the b-value is shown by the dashed line.

Figure 4.23 projects the temporal variation of b-value for the study region. The b-value is a crucial seismic characteristic, and even a slight change might have a negative impact. Here, we used the non-parametric K-S test to assess the significance of a decline in the b-value before major seismic events, in contrast to the conventional method where the change in its value was recorded without using any statistical tool. Table 4.4 lists the parameters utilized in this calculation. We use a piece of the b-value temporal curve to evaluate and validate the phenomenon of a drop in the b-value before major occurrences. According to [43], this region has seen eight moderate earthquakes with magnitudes ranging from (Mw 5.0–5.9) over the last seven months. We undertook a detailed examination of fluctuation in the slope of the b-value curve from April 2020 to October 2020, using this report as a guide, and then used the K-S test to validate the importance of the decline in b-value before any major events. The K-S test is performed with p=0.02 and p=0.05 as the significance levels. D_{max}=0.189 (Figure 4.24) is found to be the largest difference between ECDF and SCDF. It is reported that the D_{max} is more than the critical D-value thus the K–S test validates the significance of the fall in the b-values before these events.

Table 4.4: The table below includes the variables that have been utilized in the K-S significance test for the temporal variance of the b-value.

b-value	Freq	Cum Freq	ECDF	Z-Value	SCDF	D-Value
0.79	1	1	0.143	-1.415	0.079	0.065
0.8	2	3	0.429	-0.708	0.24	0.189
0.81	1	4	0.572	-0.001	0.5	0.072
0.82	2	6	0.858	0.708	0.761	0.097
0.83	1	7	1	1.415	0.922	0.079

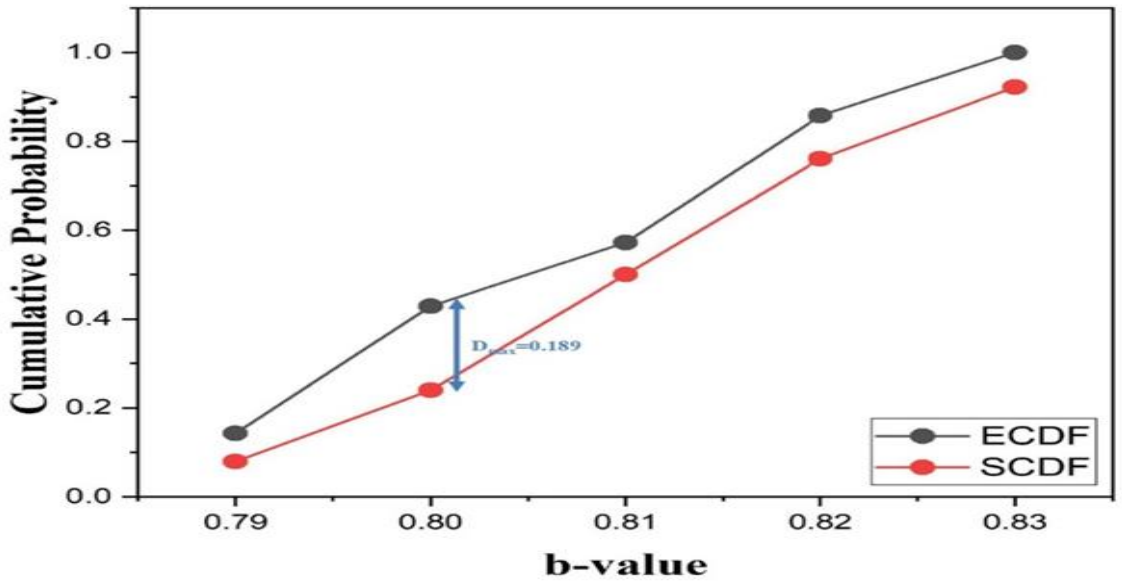

Figure 4.24: The Cumulative probability vs b-value to establish the significance of the dip in the b-value temporal curve using the K-S test is shown in the plot.

The first indication of a decline in the b-value initially surfaced in March 2020, almost two years before the primary shock, and was followed by a significant decline in the b-value in November 2020. The Mizoram earthquake consequently happened on November 26th, 2021, a few months later. With the use of the K-S test, this assertion is proven. Likewise, [44] inferred that the b-value temporal curve exhibits a drop well before the occurrence of the 2003 (M8.0) and 2008 (M7.1) earthquakes. Similarly, before the catastrophic earthquake that struck Kashmir on October 8, 2015, [45] noticed a decline in the b-value curve (Mw 7.6). Consequently, the phenomenon of a fall in the b-value as an earthquake precursor that occurs well before the main event is established in the analysis.

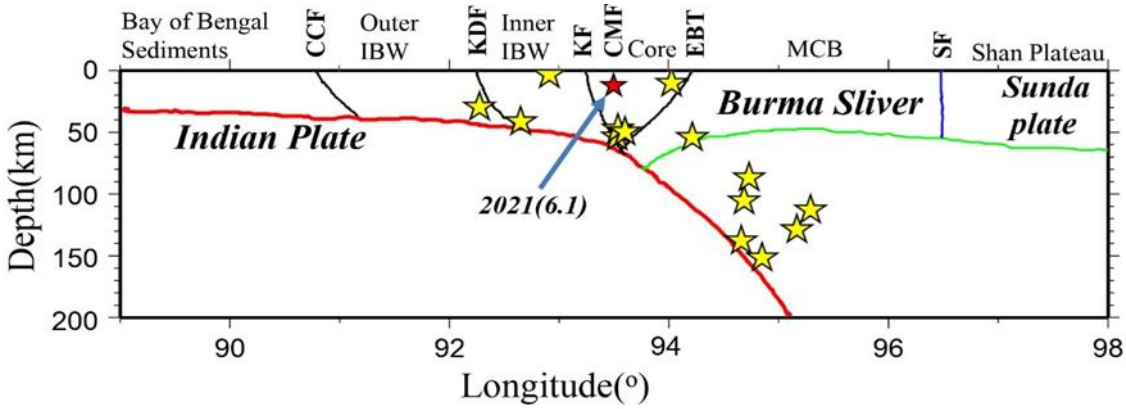

Figure 4.25: The seismotectonic model of the research area is depicted in the plot. The yellow stars indicate the epicenter of the earthquake with a magnitude $M_W \geq 6$, and the red star is the epicenter of the earthquake that occurred on November 26, 2021.

The seismotectonic model of the research area is shown in Figure 4.25, which enables us to see the active faults in the area. The interplate model aids us in estimating the location of the Mizoram earthquake (Mw 6.1) that occurred on November 26, 2021. A depth of about 12 kilometers has been reported for this interplate earthquake (as reported by the NCS, India). Figure 4.25 shows the Kopili fault, CMF, and EBT where the earthquake occurs. The depth of the earthquake with magnitude Mw ≥ 6 has been displayed in Figure 4.25 using data from the ISC-EHB catalog.

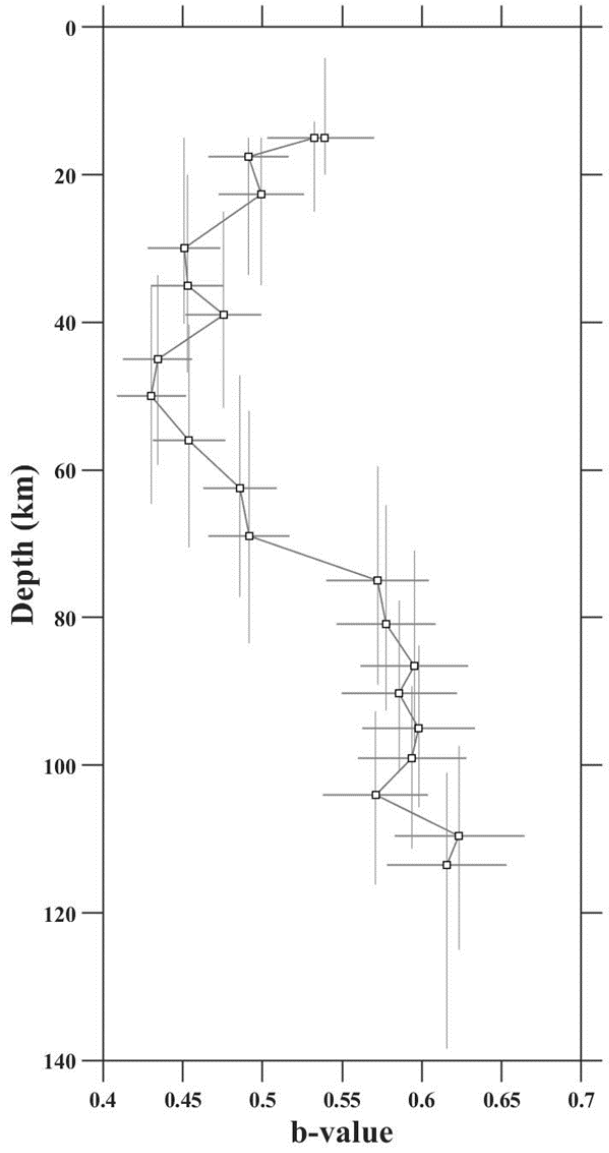

Figure 4.26: The graphic displays the depth-wise distribution in the b-value for the investigated region.

Figure 4.26 illustrates the depth-wise variation in b-values across the studied region using a dataset of 767 well-located earthquake events, primarily sourced from the ISC-EHB catalog (741 events) and GCMT (26 events). Each depth window, computed with a constant M_C and a sample window of 50 events, reveals fluctuations in b-values that aid in understanding stress accumulation beneath the Earth's crust. Earlier studies by [23] and [8] observed low b-values (0.43 to 0.55) in the upper crust (25-36 km depth), indicating localized stress concentration. The b-value sharply declines after a peak, reaching a minimum at 45 kilometers depth. For instance, the November 26, 2021 earthquake had a focal depth of 12 kilometers, influencing the b-value trends observed. Beyond 70

kilometers depth, b-values increase significantly, peaking in the 100 to 120 km range, possibly due to factors like magma chambers, reduced normal stress, groundwater interactions, or pore pressure ([46], [47], [48]). [4] attribute higher b-values in the subducted crust beneath the IBR to trapped over-pressured fluids, affecting fluid migration and heterogeneity near plate contacts. Studies by [49] and [29] suggest that deep-seated factors such as increased pore pressure and deep-lying dehydration sites contribute to elevated b-values at depths of 80-110 kilometers (Guatemala-El Salvador) and 100-150 kilometers (volcanic chains), impacting crustal stress dynamics. The significance of depth-wise b-value variance was validated using a K–S non-parametric test on a sample of 17 random b-values collected from the depth-wise b-value curve (Table 4.5), conducted at a significance level of p=0.05 and p=0.02 with n=17.

Table 4.5: The table below lists the variables used in the K-S significance test for Depth wise variation of b-value.

b-value	Freq	Cum Freq	ECDF	Z-value	SCDF	D-value
0.42	1	1	0.059	-1.205	0.115	0.056
0.425	1	2	0.118	-1.142	0.127	0.010
0.437	1	3	0.177	-0.99	0.162	0.016
0.441	2	5	0.295	-0.94	0.174	0.121
0.447	1	6	0.353	-0.864	0.195	0.159
0.453	1	7	0.412	-0.788	0.216	0.197
0.466	1	8	0.471	-0.623	0.267	0.204
0.484	1	9	0.53	-0.396	0.347	0.184
0.558	1	10	0.589	0.541	0.706	0.118
0.567	1	11	0.648	0.655	0.744	0.097
0.583	1	12	0.706	0.858	0.805	0.099
0.587	1	13	0.765	0.908	0.819	0.054
0.588	1	14	0.824	0.921	0.822	0.003
0.608	1	15	0.883	1.174	0.88	0.003
0.61	1	16	0.942	1.199	0.885	0.057
0.644	1	17	1	1.629	0.949	0.052

The maximum D-value (Dmax) as shown in Table 4.5 and Figure 4.27. Thus, the maximum D-value is found to be more than the critical D-value consequently K–S test validated the fluctuation reported in the depth-wise b-value variation.

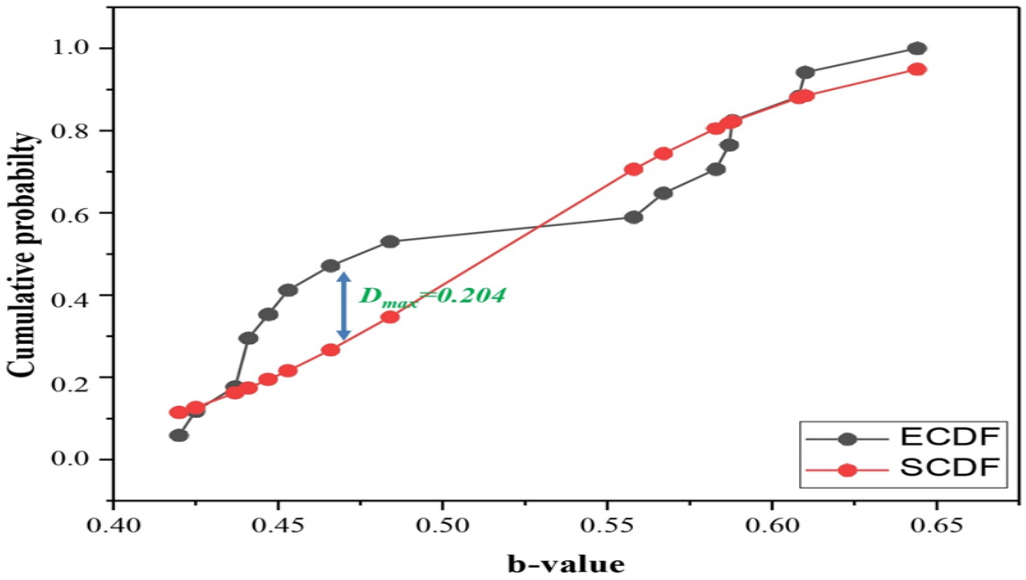

Figure 4.27: The plot illustrates the cumulative probability vs. b-value to demonstrate the significance of the depth-wise b-value fluctuation.

Figure 4.28 gives statistical data for the number of events with different depth ranges. A significant decrease in earthquake events is reported for the deep depth region (> 120km). The significant fall in the curve can be attributed to the decrease in crustal stress at the deeper depth region [8]. The comparison of the Figure 4.26 and Figure 4.28 reveals that the b-value increases as depth increases, illustrating a decreasing crustal stress character in the deeper depth zones. The depth-wise b-value implications drawn from this work apparently demonstrate a plausible association with past research that has been performed in this area ([23], [4], [8]).

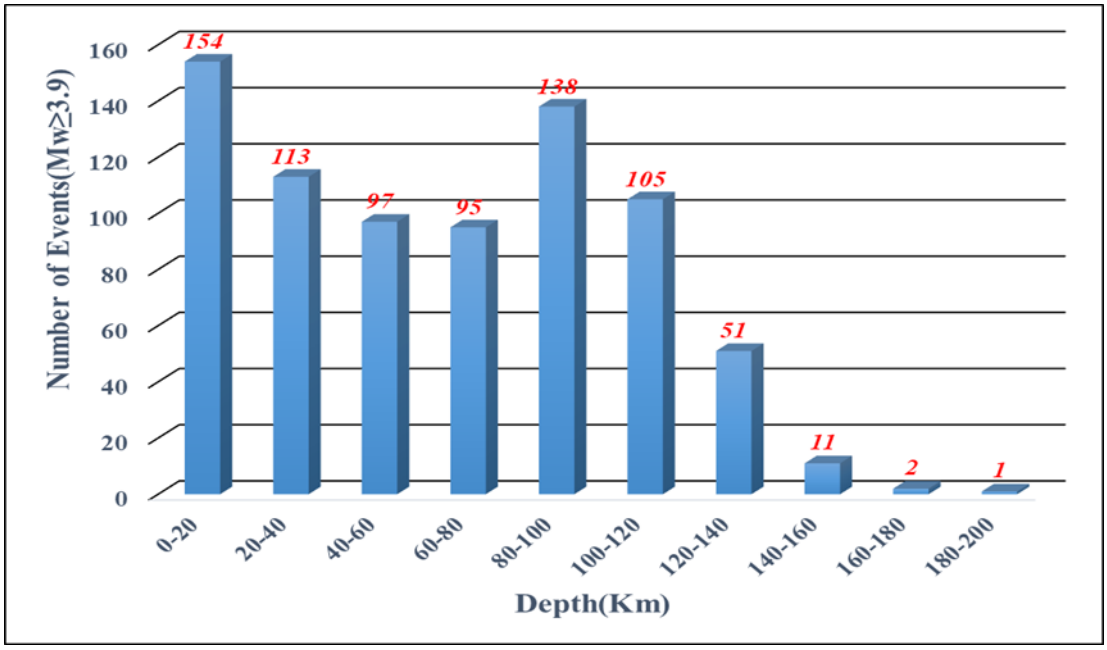

Figure 4.28: The histogram displays the depth-wise clustering of 767 earthquake events with $M_W \geq M_C$.

4.4. The Gaziantep, Türkiye Earthquake (6th February 2023, M_W 7.8)

4.4.1. Introduction

The study of earthquake precursors, particularly b-value variations and seismic quiescence (Z-value), is crucial in seismology. The b-value reflects the statistical distribution of earthquake magnitudes and varies temporally and spatially before major earthquakes. This variation can offer insights into underlying seismic processes. Seismic quiescence, a notable decrease in seismic activity, often precedes significant earthquakes. Türkiye, a seismically active region, recently experienced a major earthquake on February 6, 2023 (M_W 7.8).

This study examines spatiotemporal b-value variations and seismic quiescence before the 2023 Gaziantep earthquake (M_W 7.8), utilizing statistical methods to enhance earthquake prediction and hazard assessment.

4.4.2. Seismotectonic setup

Türkiye, situated at the intersection of the Eurasian, African, and Arabian tectonic plates, is highly seismically active due to its complex seismotectonic setup (as shown in Figure 4.29). Key active faults include the North Anatolian Fault (NAF), responsible for major earthquakes like the 1999 Marmara earthquake, and the East Anatolian Fault (EAF), site of the recent February 2023 Gaziantep earthquake (M_W 7.8) [50]. Other significant faults are the South Anatolian Fault and the Dead Sea Fault (DSF), both contributing to regional seismicity. The Bitlis-Zagros Fold Belt (BZFT) and the Lesser Caucasus (LC) and Greater Caucasus (GC) regions also exhibit intense tectonic activity due to plate interactions, including thrust faulting and subduction [51]. This intricate tectonic environment makes Türkiye prone to frequent and potentially destructive earthquakes, necessitating ongoing research to understand and mitigate seismic hazards.

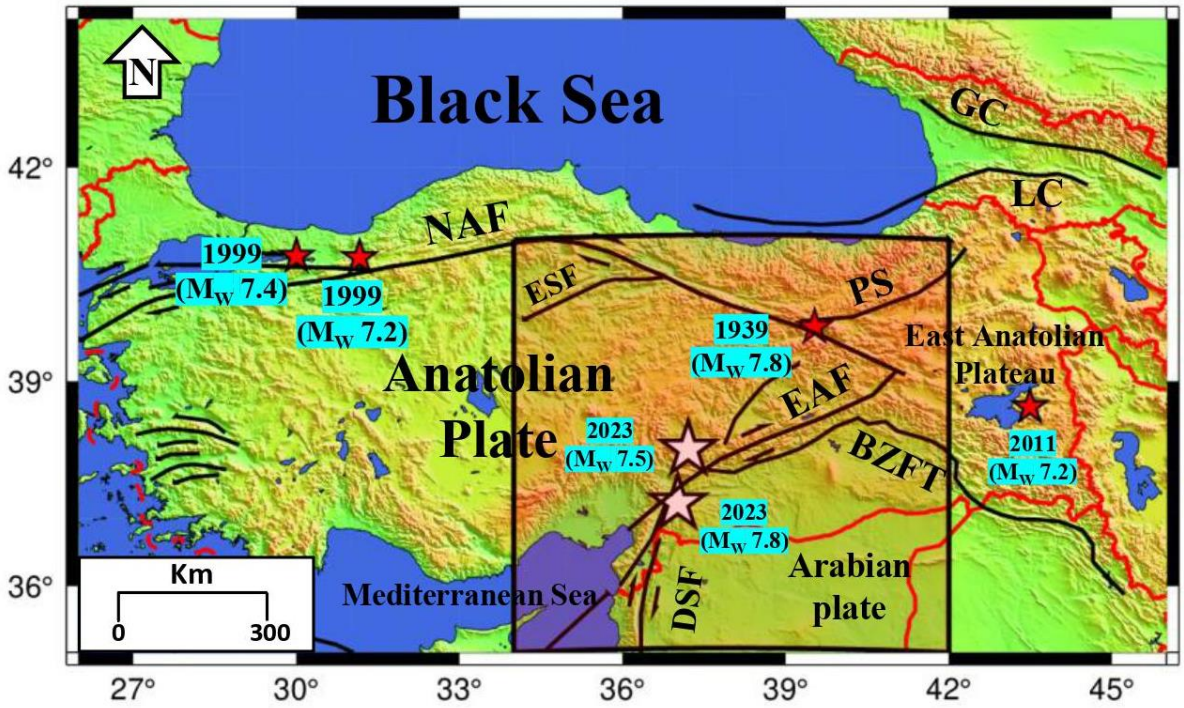

Figure 4.29: The tectonic plot of the study region. The red star shows epicentral location of 1939- Erzincan earthquake (M_W 7.8), 1999-Izmit earthquake (M_W 7.4), 1999-Duzce

earthquake (M_W 7.2), and 2011-Van earthquake (M_W 7.2). The major tectonic features include: The NAF; The EAF; The DSF; The BZFT; The LC and the GC; The Mediterranean Sea and Black Sea; Arabian plate; Anatolian plate; East Anatolian plateau. The white star shows the epicentral location of the recent 6th February 2023 Türkiye Earthquakes (M_W 7.8; M_W 7.5). The highlighted region shows the study region considered in present study.

4.4.3. Earthquake catalog and its Analysis

The study area spans 35^0 - 41^0 degrees north latitude and 34^0 - 42^0 degrees east longitude. To analyze b-value anomalies, we used a homogeneous earthquake catalog prepared by [52], covering events in Türkiye from 1905 to 2018. Additionally, data from the Kandilli Observatory and Earthquake Research Institute (KOERI), the ISC, and the USGS for events from November 1, 2018, to January 31, 2023, were utilized. These sources report magnitudes in various scales, which were converted to the M_W scale using [52] (as mentioned in Table 2.1 of chapter 2) conversion relationship. Figure 4.30 documents 89,990 seismic events (magnitudes 1.0 to 7.7 M_W) with minimal changes from 1905 to 1995 and a significant increase post-1995 due to more monitoring stations.

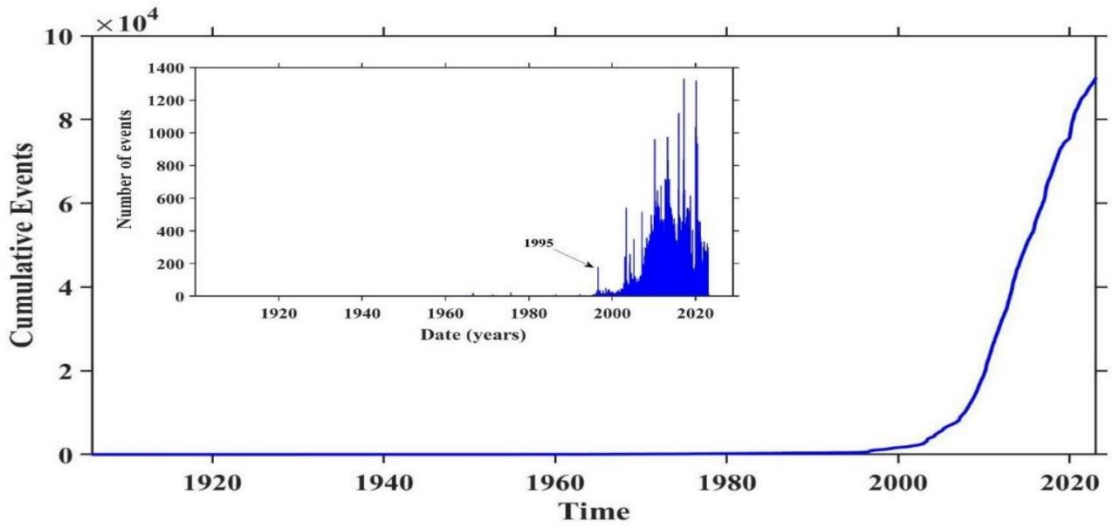

Figure 4.30: The cumulative number of events per year for the study region recorded between 1905 to 2023. The histogram illustrates the annual distribution of observed seismic events.

The catalog includes dependent events (foreshocks, aftershocks, clusters), requiring declustering to fit Poisson distribution for accurate analysis. Various algorithms (as

mentioned in Table 2.2 and Table 2.3 of chapter 2) were used, with [53] method achieving the highest declustering events (72380) (as shown in Figure 4.31).

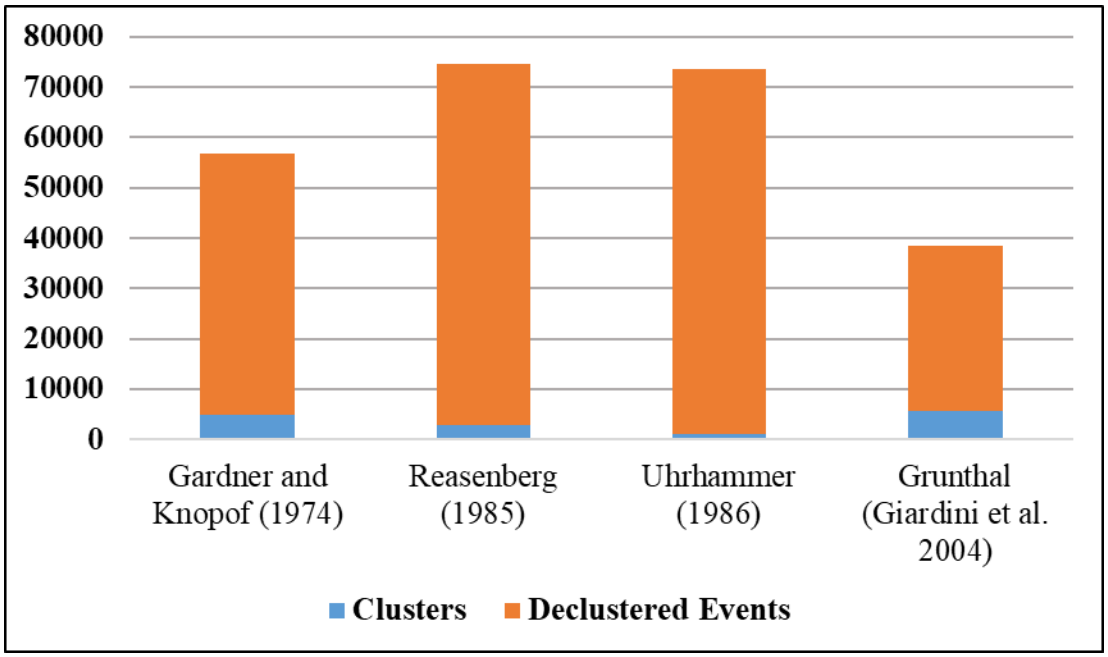

Figure 4.31: The comparative analysis of the different declustering algorithms used in this research.

To ensure the reliability of an earthquake catalog, it is crucial to assess its temporal and magnitude completeness. Methods by [54] and [55] are commonly used for this evaluation. In our study, we employed the Visual Cumulative Inspection (CUVI) method introduced by [55] to assess temporal completeness. Figure 4.32a shows that seismic activity patterns remained consistent from 1905 to 1995, with a significant increase from 1995 to 2002, followed by changes from 2002 to 2013 and 2013 to 2023. This aligns with previous studies highlighting a rise in seismic events post-1995 in the EAFZ. We affirm 1995 as the start of notable changes, concluding the catalog is temporally complete from 1995 to 2023. Figures 4.32b, 4.32c, and 4.32d depict the cumulative number, depth distribution, and magnitude distribution of events, respectively, during this period. Therefore, we consider the declustered catalog from 1995 to 2023 as complete.

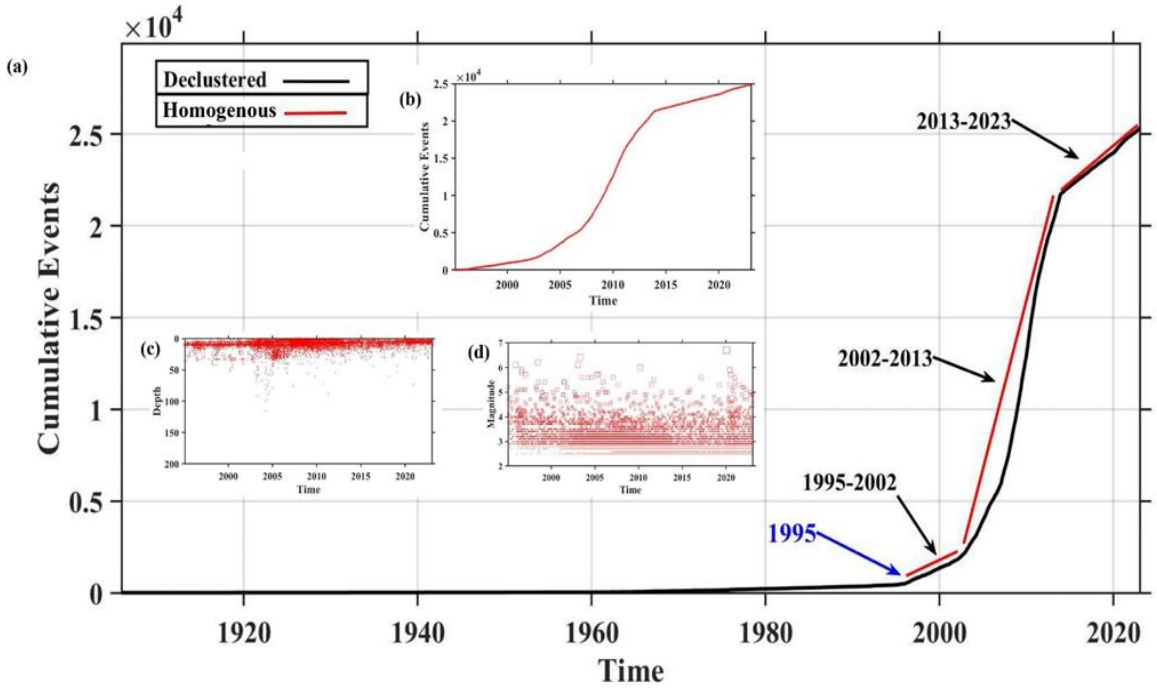

Figure 4.32: The figure presents various aspects of the earthquake catalog: (a) Cumulative declustered earthquake events catalog from 1905 to 2023, (b) Homogenous segment of the earthquake catalog spanning from 1995 to 2023, (c) Depth-wise distribution of the homogenous earthquake events, and (d) Magnitude vs. time distribution of homogenous earthquake events.

Assessing completeness involves computing the M_C to determine the smallest detectable earthquake size in a region, influenced by spatial and temporal variations. We visualize temporal changes in M_C using a sliding time frame MAXC method, with Figure 4.33 showing a range from 4.6 to 1.56 for the complete earthquake catalog. The surge in seismic activity post-1995 correlates with a decline in M_C, indicating a relationship between event count and M_C value. Recent studies support a high M_C value until 1995, followed by a decline, particularly in the EAFZ ([56], [57], [58]).

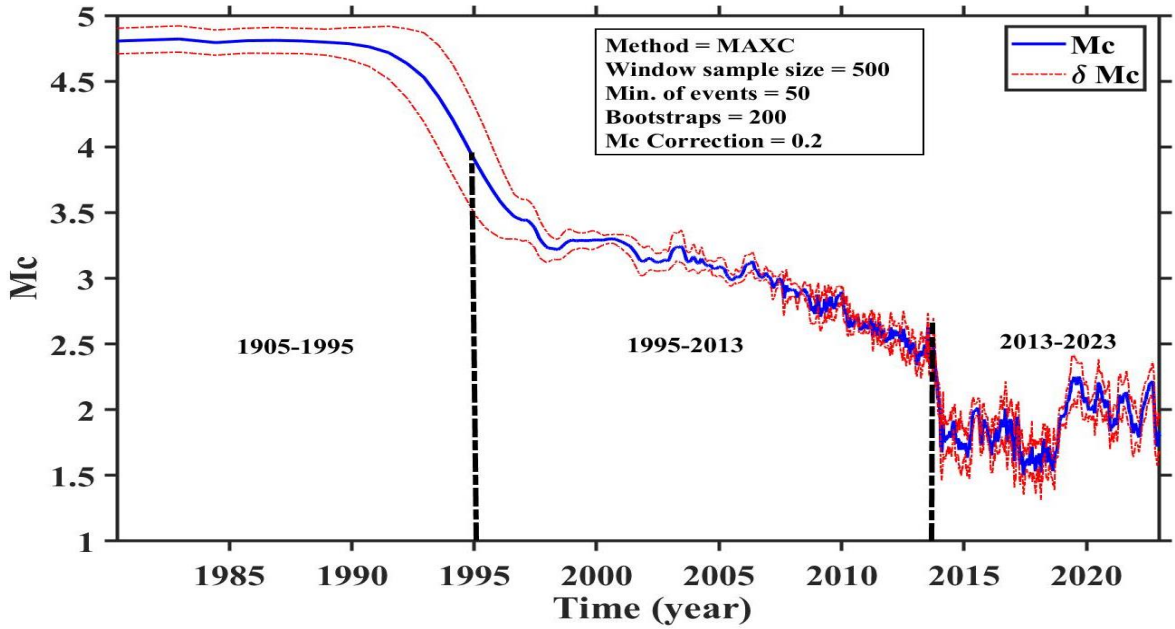

Figure 4.33: The Time-dependent changes in the M_C for the study region. The SD in M_C value is illustrated by the red dashed line.

To enhance M_C analysis, the complete catalog was divided into two periods: 1905 to 1995 and 1996 to 2023. Using a grid with 0.2-degree dimensions, the spatial distribution of M_C was computed, employing the MAXC method [34] with a correction factor of '+ 0.2' [35]. Figure 4.34(a-b) illustrates a high M_C value from 1905 to 1995 and a significant decrease from 1995 to 2023. Seismic station proliferation in recent years ([59], [52]) has enabled the recording of minor seismic events, impacting M_C values.

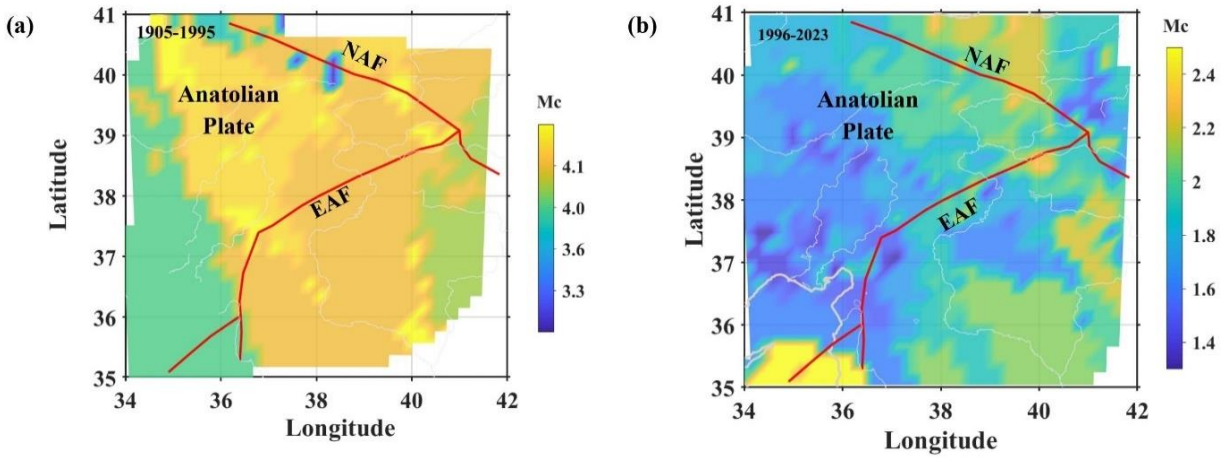

Figure 4.34: The figure illustrates the geospatial distribution of the M_C for the study region during two distinct periods: (a) 1905-1995 and (b) 1995-2023.

Figure 4.35 indicates an overall M_C of 2.5, signifying completeness in magnitude for earthquakes with a magnitude of 2.5 or higher.

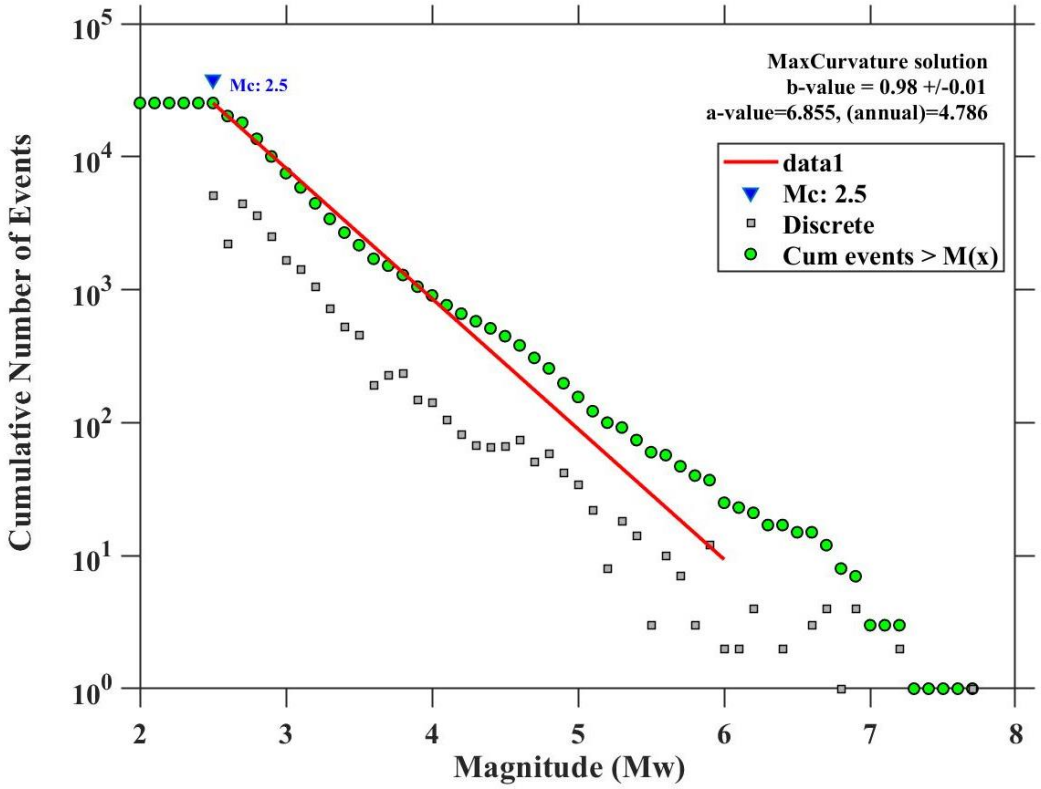

Figure 4.35: The FMD curve for the study region.

After confirming temporal completeness from 1995 to 2023 with an M_C value of 2.5, we proceeded with further analysis. Figure 4.36 illustrates the spatial and depth distribution of uniform earthquake events. Notably, most events are concentrated in the upper crust region. Additionally, a recent earthquake in Gaziantep on February 6th, 2023, with M_W 7.8 at a depth of 10 km, provides valuable insight into regional seismic activity, enhancing our understanding of the earthquake catalog.

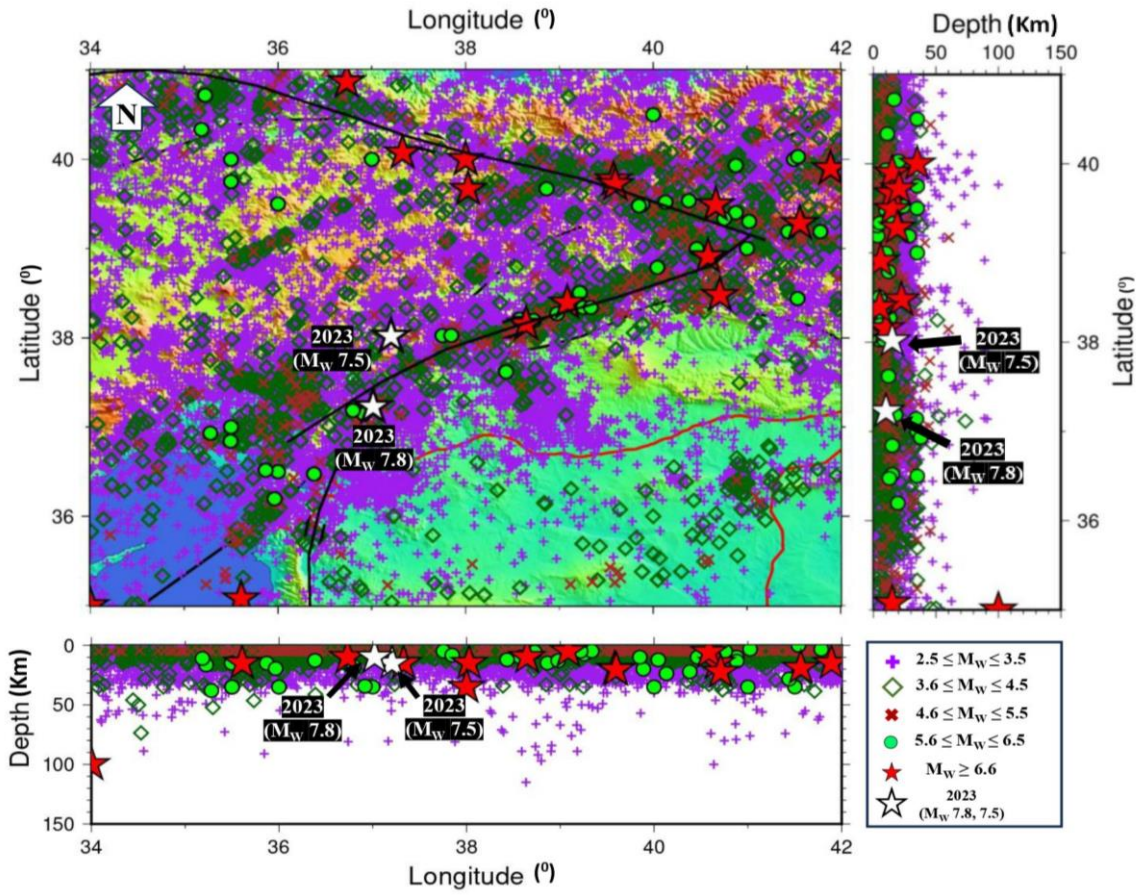

Figure 4.36: The epicentral location of the declustered homogenous earthquake events having magnitude $M_W \geq M_C$. The white stars depict the epicentral location of recent 6th February 2023 Türkiye Earthquakes (M_W 7.8 and 7.5).

4.4.4. Methodology Adopted

This study employs the modified MLE approach proposed by Aki and Utsu, known as the Aki-Utsu MLE ([14], [15]) to analyze seismic activity. Furthermore, the SD in b-value is determined by applying the formula proposed by [16]. The average b-value derived from this method is b=0.98 ± 0.1, as illustrated in Figure 4.35.

4.4.5. Results and Discussion

For meticulous seismic investigation, the entire research area is divided into 12 uniformly spaced grids, and GR parameter (b-value) for each grid is determined. In order to maintain the natural grid-to-grid continuity of data points, we have maintained the original size of each subregion at 2^o x 2^o and chosen a moving window with dimensions of 1^o x 1^o.

Table 4.6: The value of the GR parameters for each grid is listed in the table.

S.no	Longitude (^{0})	Latitude (^{0})	b-value	δb	Number of Events
1	34-36	35-37	0.74	0.02	1203
2	34-36	37-39	1.12	0.02	2497
3	34-36	39-41	1.01	0.02	2398
4	36-38	35-37	1.11	0.03	1518
5	36-38	37-39	0.86	0.02	3979
6	36-38	39-41	0.88	0.02	1683
7	38-40	35-37	1.06	0.08	343
8	38-40	37-39	0.94	0.01	6001
9	38-40	39-41	1	0.02	3205
10	40-42	35-37	0.6	0.02	358
11	40-42	37-39	0.87	0.02	1772
12	40-42	39-41	0.84	0.01	4434

The illustration of the geospatial variation of the b-value for the region under consideration is shown in Figure 4.37. The b-value for each grid is estimated using the MLE technique developed by [14] and refined by [15], sometimes referred to as the Aki-Utsu ML method. Table 4.6 presents the range of b-values obtained in the research area, spanning from 0.6 to 1.12. In a recent study conducted by [58] on the Eastern Anatolian zone of Türkiye a range of b-values from 0.66 to 1.60 was reported. Therefore, the b-values observed in the current study align with the earlier findings. Furthermore, [16] proposed an estimation method for the SD observed in the b-value estimation, and Table 4.6 shows its spatial distribution. In this chapter, the low b-value is observed along the EAFZ, and South-eastern Anatolia Region. The EAFZ, situated in eastern Türkiye, is a significant fault system that serves as the boundary between the Anatolian Plate and the Arabian Plate. The recent earthquake that occurred on February 6, 2023, near Gaziantep, Türkiye, with a magnitude of M_W 7.8, took place in close proximity to this fault zone. Similarly, The South-eastern Anatolia Region, also known as South-eastern Türkiye, is in the south-eastern part of the country. This region is seismically active and experiences frequent earthquakes due to its tectonic setting. The epicentral location of the recent earthquake occurred on 6th February 2023

Gaziantep, Türkiye Earthquake (M_W 7.8) is found to be in an b-value grid (b < 1). In the recent studies it has been observed that the regions positioned at low b-value zones have high potential of future earthquakes ([8], [4]). According to a study conducted by [59], it was noted that lower b-values are indicative of higher stress release. Consequently, the occurrence of the 6th February 2023 Gaziantep, Türkiye Earthquake (M_W 7.8) in an area with low b-values may suggest a lower level of accumulated strain resulting from subduction tectonics. This implies that stress gradually accumulates over time and is subsequently released through less frequent, yet more significant, earthquake [60]. [61] conducted a study and found that the epicenter of the 1999 Izmit earthquake (M_W 7.4) was situated in a region with a low b-value. Similarly, [62] reported a low b-value around the epicenter of the 2011 Van-Erciş earthquake in Türkiye, which had a magnitude of 7.2. On a global scale, [8] discovered that the epicenter of the 2016 Manipur, India earthquake, with a magnitude of 6.7, was located in an area with intermediate b-values. Furthermore, [63] reported that the epicenter of the 2004 Sumatra earthquake (M_W 9.0) was in a region with relatively low b-values. Therefore, based on the aforementioned discussion, it can be inferred that the occurrence of the February 6, 2023 Gaziantep, Türkiye earthquake (M_W 7.8) in a low b-value region indicates a significant accumulation of stress prior to its occurrence. Additionally, the current analysis of b-values demonstrates a plausible correlation with the earlier studies.

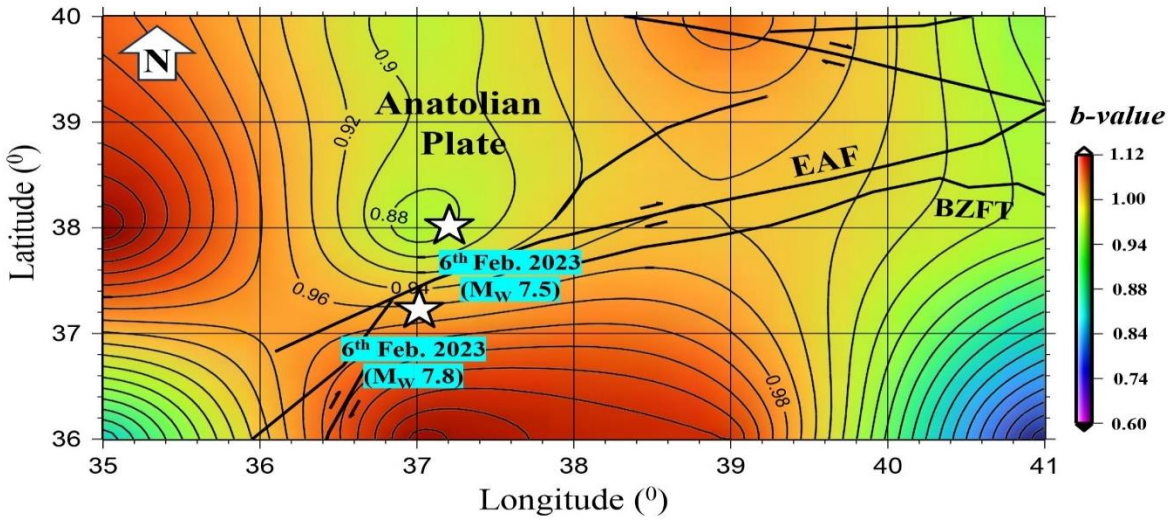

Figure 4.37: The geospatial distribution of b-value for the study region. The epicentral location of 6th February 2023 Gaziantep, Türkiye Earthquake (M_W 7.8) is represented by black star.

The significance of conducting a comprehensive study on b-value variation using statistical tools was not fully recognized in previous research, which predominantly relied on traditional methods of visual inspection. Consequently, the importance of systematically analysing b-value variations using statistical techniques was underestimated. Due to the existing gaps in prior research, this article aims to address them by conducting a comprehensive seismic analysis of the spatial disparity in b-values leading up to the February 6, 2023 Gaziantep earthquake in Türkiye (M_W 7.8). The analysis is performed using the K-S nonparametric test. The advantage of nonparametric analysis lies in its ability to make fewer assumptions about the data, require a smaller sample size, and become necessary when data can be ranked but lacks clear numerical interpretation, such as in the case of assessing preferences. The K-S test involves the use of the ECDF, SCDF, and Z-value. The ECDF represents the empirical distribution of a dataset, while the SCDF standardizes it for easier comparison and analysis. The Z-value quantifies the maximum vertical deviation between the ECDF and the hypothetical distribution, indicating a larger discrepancy between the observed data and the hypothesized distribution. The parameters used for the K-S test have been listed in the Table 4.7.

Table 4.7: The K-S parameters used to examine the geospatial variation of b-value for the EAFZ.

b-value	ECDF	Z-value	SCDF	D-value
0.6	0.059	-2.458	0.007	0.052
0.74	0.118	-1.566	0.059	0.059
0.84	0.176	-0.928	0.177	0.001
0.86	0.235	-0.8	0.212	0.024
0.87	0.294	-0.737	0.231	0.063
0.88	0.353	-0.673	0.25	0.102
0.94	0.412	-0.29	0.386	0.026
1	0.588	0.092	0.537	0.052
1.01	0.647	0.156	0.562	0.085
1.06	0.882	0.475	0.682	0.200
1.11	0.979	0.693	0.683	0.296
1.12	1	0.857	0.804	0.196

The K-S test is utilized to assess the statistical implication of the spatial dispersion of b-values. Table 4.7 contains the parameters used in the K-S test, which can be referenced for more details. By employing a significance level of p = 0.2 and analyzing a total sample size of 15, it was observed that the maximum D-value exceeded the critical D-value, as depicted in Figure 4.38. Consequently, the null hypothesis is rejected, implying that there is a significant difference in the geographical distribution of b-values.

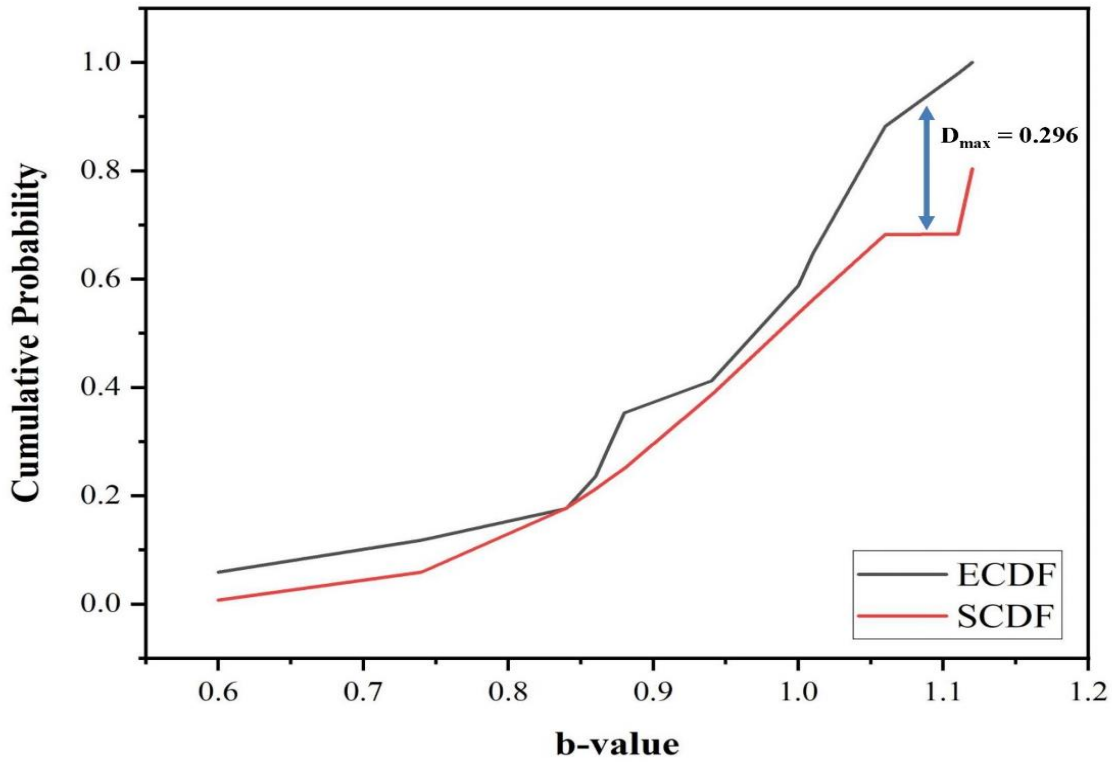

Figure 4.38: The plot depicts the difference between the ECDF and SCDF to examine the geospatial variation of b-value.

When studying seismicity, researchers (such as [64], [58], [8], [65] etc.) commonly examine the changes in the b-value parameter over time. Typically, earthquake data is analyzed using a power-law distribution assumption. Analyzing the variations in the b-value over time provides insights into seismic activity and stress levels within a specific region. An increase in the b-value indicates a higher occurrence of smaller-magnitude earthquakes, suggesting a period of heightened seismic activity or stress release. Conversely, a lower b-value may indicate a period of increased stress accumulation or the potential for more significant earthquakes. Therefore, examining the changes in the b-value parameter over time is crucial in seismic analysis, as it helps researchers understand seismic activity, stress variations, and potential earthquake hazards within a given region.

To investigate the temporal changes in the b-value, it is necessary to utilize a long-term earthquake catalog and employ appropriate statistical methods to identify significant variations. There are various methods to evaluate temporal fluctuations in the b-value before major earthquakes. These include sliding window analysis, time-dependent rate models, cumulative number of earthquakes, Bayesian methods, GR Variability analysis, and statistical hypothesis testing. These methods help identify and quantify temporal variations in b-value, providing insights into seismic activity patterns and potential earthquake hazards. By applying these methods to long-term earthquake catalogues, researchers can better understand seismic activity patterns and potential hazards. However, in order to fully grasp the seismic behaviour in a given region, it is necessary to take additional seismic parameters into account and conduct in-depth analyses. To accurately analyse the temporal fluctuation of the b-value, it is important to account for the heterogeneity of the Earth's crust. In this regard, we focus specifically on the seismic events that occurred within the square grid delineated by 36^0-38^0 E longitude and 37^0-39^0 N latitude, which coincides with the epicentral location of the February 6, 2023 Gaziantep earthquake in Türkiye with a magnitude of M_W 7.8. By narrowing our analysis to this specific region, we can mitigate the potential impact of crustal heterogeneity and ensure a more precise examination of the temporal changes in the b-value. Figure 4.39 presents the temporal fluctuation of the b-value prior to the Gaziantep earthquake epicenter in Türkiye, which took place on February 6, 2023, with a magnitude of 7.8. This Figure 4.39 provides insights into how the b-value changed in the vicinity of the earthquake epicenter from 2020 to 2023. We estimate the temporal variation in the b-value using the MAXC approach by employing the Moving Window method with a sample of 500 events. Furthermore, we enhance the estimation using bootstrapping, a resampling technique conducted 200 times to ensure the robustness and reliability of the results. This methodology yields valuable insights into how the b-value, a critical parameter in seismicity analysis, varies over time, providing a comprehensive view of the seismic activity in the region. The temporal analysis of the b-value reveals a general downward trend leading up to the February 6, 2023 Gaziantep earthquake in Türkiye with a magnitude of 7.8. Likewise, the decline in b-value for other notable events occurring in the study region can be observed from the Figure 4.39. Similar conclusions were drawn by [40] in the case of the Sumatra earthquakes in 2002 and 2004, and by [66] before the devastating Wenchuan earthquake (Mw 8.0) in southwest China in 2008. [66] specifically studied the b-value changes in southwest China and suggested that the gradual decrease in

the b-value between 2000 and 2008 could be interpreted as a precursor to the Wenchuan earthquake. The b-value slope was also observed to be negative prior to the massive earthquakes that struck the Pacific coast of Tokachi, Hokkaido, Japan on September 26, 2003 (M8.0) and September 11, 2008 (M7.1), as reported by [44]. Furthermore, [67] found similar results for the southern California region, establishing a correlation between low b-values and mainshocks. Numerous studies, such as [8] and [68], have identified that fluctuations in the b-value at a seismic site can serve as a predictive indicator for the occurrence of large or moderate earthquakes in the near future. The temporal curve of the b-value for the analysed region, as shown in Figure 4.39, demonstrates a decline in its value well before the occurrence of the February 6, 2023 Gaziantep, Türkiye earthquake (M_W 7.8). In a recent study conducted by [63], the relative analysis of the temporal fluctuation in the b-value was utilized. Similarly, in this chapter, the same method was implemented to examine the temporal discrepancy of the b-value and determine the percentage decrease in the b-value leading up to the main event. The highest and lowest b-values observed in the temporal curve were used to calculate the percentage fall in the b-value. In Figure 4.39, the highest b-value occurred approximately 2.5 years before a decline in the b-value was observed prior to the occurrence of the February 6, 2023 Gaziantep, Türkiye earthquake (M_W 7.8). The formula employed to calculate the relative b-value is as follows:

$$\frac{\Delta b}{b} = \frac{b_2 - b_1}{b_2} \times 100$$

where, the b_1 is b-value at time t_1 and b_2 is the b-value at time t_2. Here, the b_2 = 1.03 and b_1=0.702. The relative fall in b-value is found to be 32 % before the occurrence of the 6th February 2023 Gaziantep, Türkiye Earthquake (M_W 7.8).

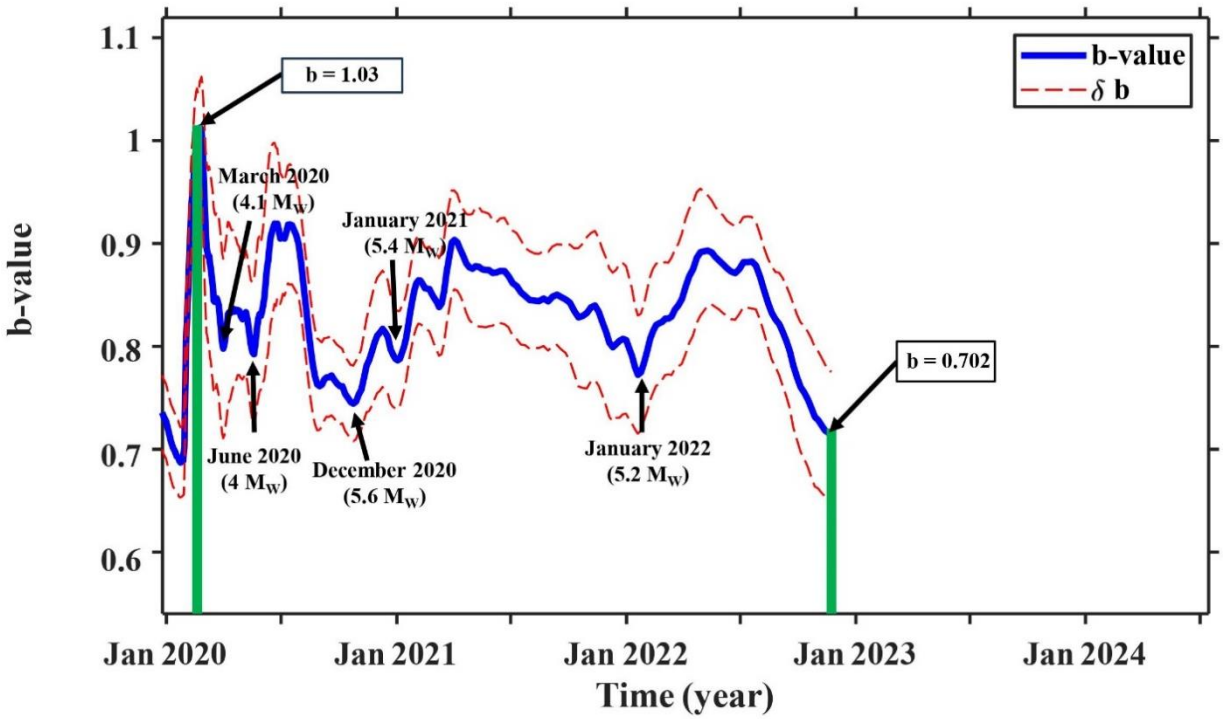

Figure 4.39: The temporal fluctuation of b-value before the occurrence of 6th February 2023 Gaziantep, Türkiye Earthquake (M_W 7.8).

4.4.5.3. b-value variation with depth

The variation of b-values with depth is an important aspect to consider when studying seismicity in a specific region ([47], [4], [69]). The b-value is known to exhibit changes with depth, and these variations can provide insights into the underlying seismogenic processes. In general, b-values tend to decrease with increasing depth. This means that the ratio of small to large earthquakes decreases as we go deeper into the Earth. The reasons for this depth-dependent variation are not fully understood and can vary from region to region. The stress regime and rock properties can change with depth, influencing the behavior of earthquakes. At shallow depths, where the stress conditions are relatively lower, faults may be more prone to small-scale slipping, resulting in a higher b-value. As depth increases, the stress levels typically increase, favoring larger earthquakes and reducing the b-value ([46], [8]). Likewise, the frictional characteristics of fault zones can vary with depth. At shallower depths, fault surfaces may have higher roughness and be more irregular, allowing for a greater number of small-scale seismic events (higher b-value). Deeper fault zones may exhibit more smooth surfaces with stronger interlocking, promoting larger-scale earthquakes (lower b-value). The physical properties of rocks, such

as their composition and deformation history, can vary with depth. Heterogeneous structures can lead to variations in stress concentration, fault strength, and seismic behaviour. These variations can influence the b-value at different depths [4]. It has been observed that the depth-dependent variation of b-values is not universal and can differ from region to region. Some regions may show a gradual decrease in b-value with depth, while others may exhibit more complex patterns with distinct changes at specific depths. Additionally, the accuracy and quality of seismic data at different depths can also affect the estimation of b-values. Incorporating information from geophysical surveys, borehole data, and geological studies can also contribute to a more detailed understanding of the depth-dependent seismicity patterns in a particular region. It can be observed from the Figure 4.40 that the b-value for the study region varies from 0.7 to 1.01 (as shown in Figure 4.40). The horizontal lines show the SD observed in b-value while vertical lines show the SD observed in the depth estimation (as Shown in Figure 4.40). The striking peak has been observed for the depth range 5 to 10 km and followed by a sharp decline in b-value. This peak in b-value for these depth ranges can be attribute to the high proportion of large magnitude earthquake as compared to small magnitude earthquakes. The low b-value observed for the depth range can be attributed to the fact of stress accumulation in the lower depth region. The focal depth of the 6th February 2023 (Mw 7.8) is found to be 10 km that falls in the high b-value bin. Moreover, it can be inferred from the Figure 4.41 that most of the seismic activities are confined in the upper depth region (5 to 10 km) depth range and very less seismic activity is observed in the deeper depth region.

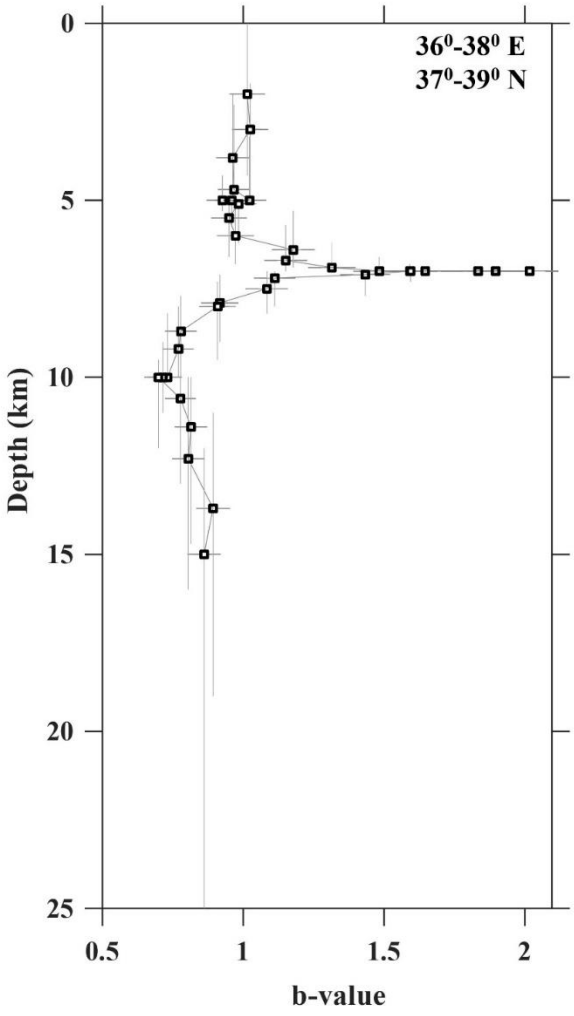

Figure 4.40: The depth wise b-value variation for the study region is plotted in the figure.

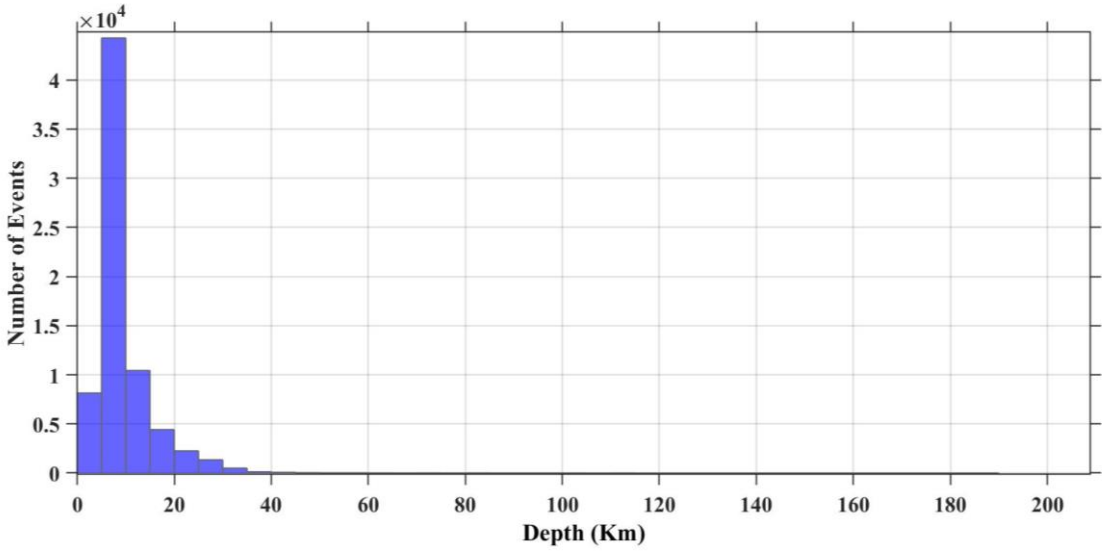

Figure 4.41: The depth wise distribution of earthquake events observed in the study region.

In the present analysis, we have observed a diminishing b-value with increasing depth. [4] have also made similar implications for the Indo-Burma subduction region. Moreover, while analyzing the anomalous behavior of b-value ([46], [47], [48]) implicates that the high b-value observed in deeper region can be attributed to the groundwater interaction or pore pressure, normal stress reduction and formation of magma cambers deep inside the earth's crust. Pore pressure is the term used to describe the pressure that fluids within rocks or fractures apply. When fluids, such as water or hydrocarbons, inflow into or build up in subterranean formations, elevated pore pressure can result. Because of the higher fluid pressure, faults may experience less effective stress, which increases the likelihood that they would slip and cause earthquakes. Due to the predominance of smaller, more frequent seismic events, higher b-values can be seen in regions with increased pore pressure. When the tectonic pressures operating on a fault decrease, the typical stress reduction takes place. This may occur for several reasons, including as interactions at plate boundaries or the release of accumulated stress through seismic activity. A higher b-value can arise from a higher proportion of smaller earthquakes relative to larger ones when the usual stress lowers. Likewise, volcanic activity or the existence of a magma chamber can potentially affect the b-value. Increased seismic activity can result from magma intrusion or movement beneath the Earth's surface because it can distort the nearby rocks and alter their stresses. The quantity of minor volcanic earthquakes linked to magma movement and volcanic processes might cause a higher b-value in volcanic zones. Since the epicentral location of 6th February 2023 (M_W 7.8) has been observed near the Eastern Anatolian Plate which is a part of the larger Anatolian Plate, that is being squeezed between the Eurasian Plate to the north and the Arabian Plate to the south. The collision between these two plates has led to the uplift of the Anatolian Plate, resulting in the formation of the Eastern Anatolian Plateau. Studying the variation of b-values with depth requires a comprehensive earthquake catalog that includes events at various depths, along with robust statistical methods. Thus, we have applied the K-S non-parametric test to testify the depth wise variation of b-value for the study region. The b-value is used to characterize the seismicity of a region. It describes the relationship between the magnitude of earthquakes and their frequency of occurrence. The K-S nonparametric test can be applied to analyze the depth-wise b-value distribution in seismic data. The b-value against each depth bin of 5km is recorded and once the b-value for each depth bin has been estimated, we define the null hypothesis and alternative hypothesis for the depth-wise b-value distribution. The null hypothesis could be that the b-values are the same across all depth intervals, while the

alternative hypothesis could be that there are significant differences in b-values between different depth intervals. After applying the K-S nonparametric test to compare the b-value distributions at different depths, we compare the calculated test statistic against critical values from the K-S distribution. At significance level p = 0.2, the test statistic exceeds the critical value (as shown in Figure 4.42); thus, we rejected the null hypothesis and concluded that there are significant differences in the depth-wise b-value distribution. The K-S nonparametric attributes used to perform depth-wise b-value calculations are listed in the Table 4.8.

Table 4.8: The table lists the K-S Test Results for depth wise b-value variation.

b-value	ECDF	Z-value	SCDF	D-value
0.7	0.077	-2.116	0.018	0.06
0.8	0.154	-1.037	0.151	0.004
0.86	0.231	-0.389	0.349	0.119
0.89	0.308	-0.065	0.475	0.167
0.91	0.385	0.152	0.561	0.176
0.96	0.462	0.691	0.756	0.294
0.97	0.77	0.799	0.788	0.019
1.01	1	1.231	0.891	0.11

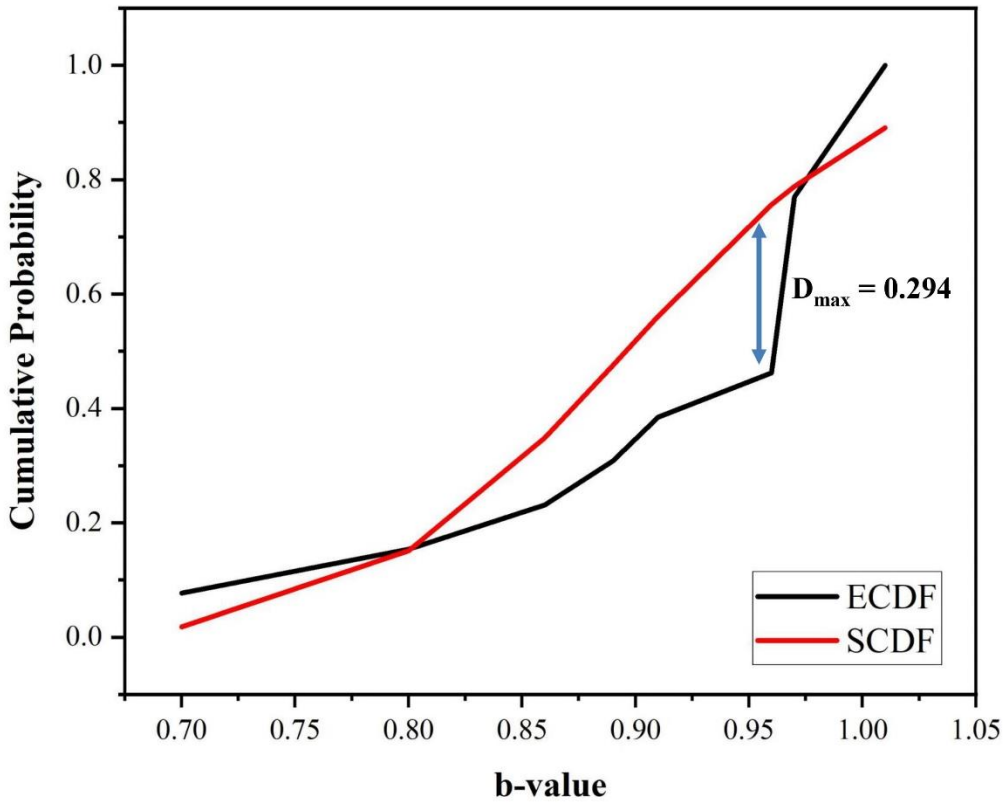

Figure 4.42: The K-S nonparametric test plot showing the difference between the ECDF and the SCDF to examine the depth wise b-value variation.

By applying the K-S nonparametric test to the depth-wise b-value distribution, we can gain insights into potential variations in seismic activity at different depths. This analysis can help understand the seismotectonic characteristics of a region and provide valuable information for seismic hazard assessment.

4.5. The Nepal earthquake (9th November 2022, M_W 6.3)

4.5.1. Introduction

Nepal, located in the Himalayan belt due to plate collision, faces high earthquake risk. The convergence of the Indian and Eurasian plates along the India-Nepal border generates seismic activity. Nepal's fault systems, including the MBT, MCT, and MFT, have caused major earthquakes [70] (as shown in Figure 4.43). Historical events, like those in 1505, 1833, 1934, and 2015, led to significant casualties and damage, with the 2015 Gorkha earthquake causing thousands of deaths [71]. Nepal has experienced around 206 earthquakes with $M_W \geq 5$ since 1826 [72]. As one of the most earthquake-prone countries, Nepal's seismicity is analyzed using statistical techniques in this chapter. The GR method [2] is used to assess seismicity through the b-value, indicating major to minor earthquake ratios. This chapter aims to analyze the b-value before the November 9, 2022 earthquake (M_W 6.3) in terms of space, time, and depth. Unified earthquake data from ISC and USGS is utilized. Despite previous investigations, the b-value's statistical importance was overlooked. We conducted a detailed analysis of its spatio-temporal and depth-wise variations, supported by the K-S test.

4.5.2. Tectonic setup

Nepal's seismic risk is high due to its location where the Indo-Australian and Asian plates converge, leading to frequent seismic activity (Figure 4.43). The collision of the Indian and Eurasian plates formed the Himalayas and causes the subduction of the Indian Plate beneath the Eurasian Plate, generating earthquakes. Various fault zones, including the MCT, MBT, and MFT, contribute to seismic activity in the region [73]. The Indus-Yarlung Suture Zone (IYSZ) marks the boundary between the Indian and Eurasian Plates, with additional faults like the Motihari Gauri Shanker fault (MG) and Karnali fault (KF) contributing to seismic landscape complexity.

These faults, including the Motihari Everest fault (ME), Arun fault (AF), and Kanchenjunga fault (KANF), alongside lineaments like the Judi fault (JF) and Thaple fault (TF), delineate the intricate tectonic processes in eastern Nepal. The geological landscape, shaped by these fault lines, underscores the region's vulnerability to seismic events.

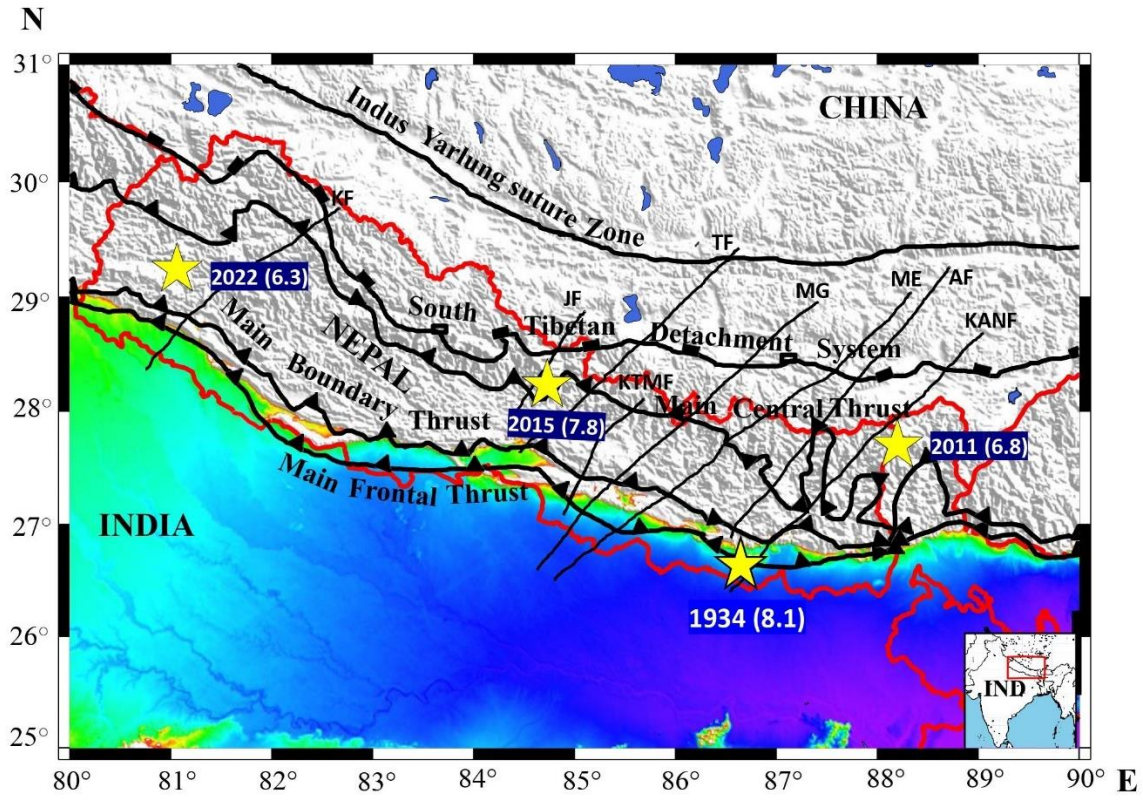

Figure 4.43: The tectonic plot of the study region. Yellow star shows epicentral location of 1934 (8.1), 2011 (6.8), 2015 (7.8) and 2022 (6.3) earthquake. The seismic entities include: The MCT; The MBT; The MFT; The South Tibetan Detachment System (STDS); KTMF; The IYSZ; KF; AF; JF; ME; TF; MG; KANF. The inset map is also attached showing study region.

4.5.3. Data Analysis

Catalogs are essential for seismic research, aiding in identifying seismic sources and assessing earthquake hazards. We compile an earthquake catalog spanning 1900 to 2022 for the area between latitudes 26° and 32° N and longitudes 80° and 90° E from ISC and USGS, comprising 3888 events with Magnitude $M_W \geq 3.5$. To ensure accuracy, we decluster the catalog, removing dependent events like foreshocks and aftershocks, using

the [11] (as mentioned in Table 2.2 of chapter 2) algorithm with default as implemented in Zmap [21]. The declustered events are depicted in Figure 4.44.

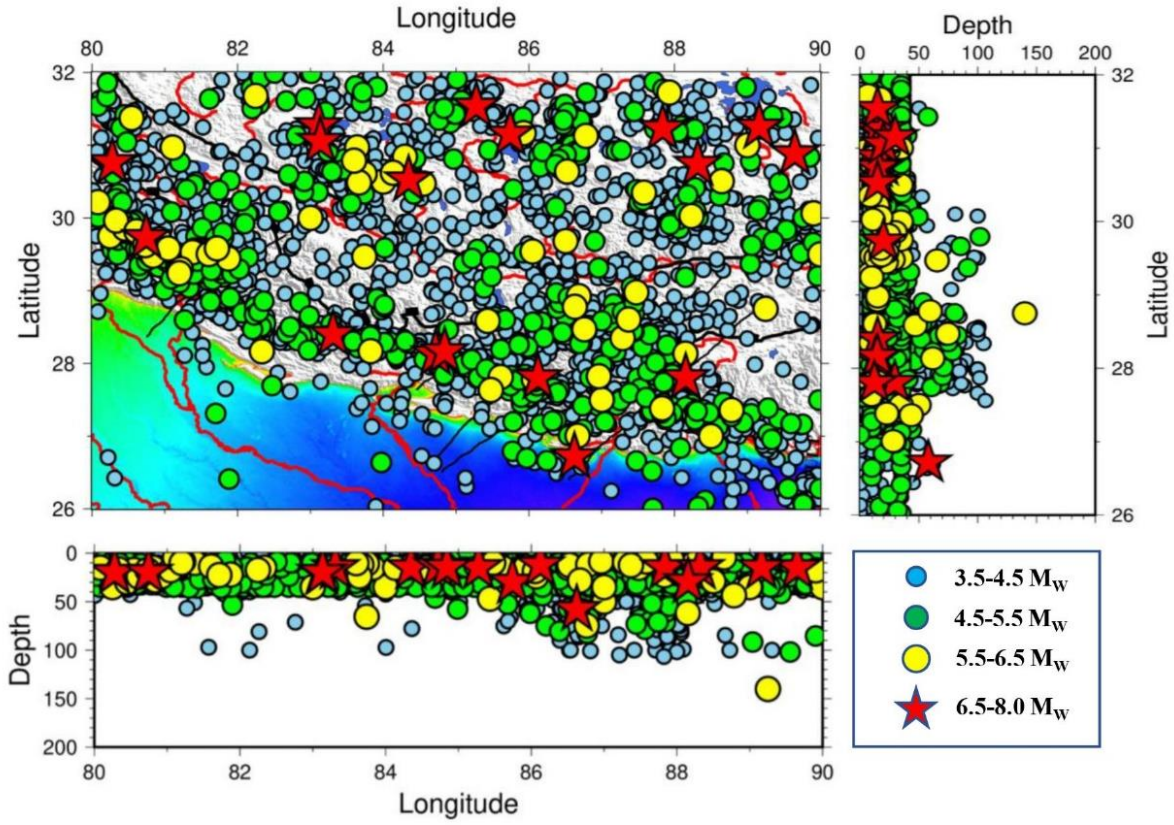

Figure 4.44: The plot shows the epicentral location of all the declustered events (2174) with magnitude $M_W \geq 3.5$.

The earthquake catalog comprises events from ISC and USGS with varying magnitude scales: mb, M_S, M_D, M_L, and M_W. To standardize, all magnitudes are converted to M_W utilizing conversion equations by [12] and [74] (as mentioned in Table 2.1 of chapter 2). After converting the whole dataset into a uniform and homogeneous database, M_C is calculated using the MAXC algorithm [34]. The temporal fluctuation of M_C is best seen in Figure 4.45.

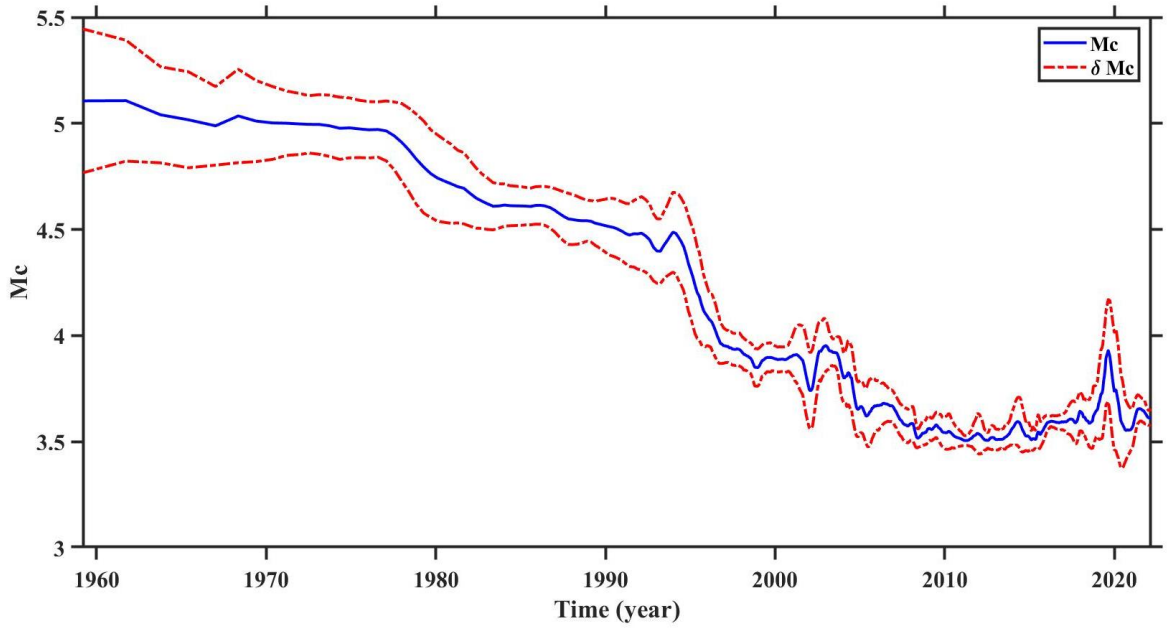

Figure 4.45: The fluctuation in the M_C across time. The dotted lines signify the observed SD in the M_C.

As shown in Figure 4.46, the average value of the M_C for the study area is 3.7. As a result, earthquakes with magnitudes $M_W \geq 3.7$ are deemed to be fully represented in the catalogue.

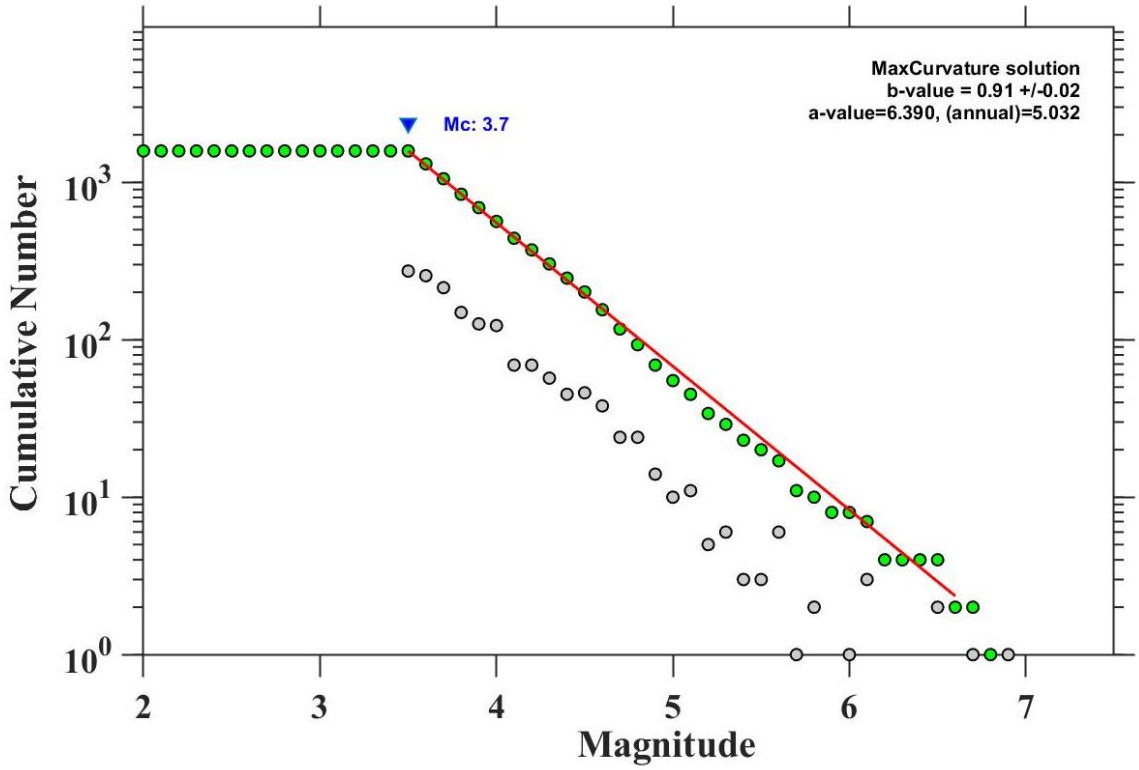

Figure 4.46: The FMD curve for the study region. The average b-value and the M_C is also mentioned in the plot.

4.5.4. b-value estimation

This study employed the Aki-Utsu MLE ([14], [15]) to approximate the mean b-value for the research area, with standard deviation estimates obtained using the formula developed by [16]. The average b-value derived from this method is b=0.91± 0.2, as illustrated in Figure 4.46. To examine spatial variation, the research area was divided into sixteen grids, and a moving window approach was employed. The Zmap tool [21] was used to compute the b-value for each grid. Additionally, the non-parametric K-S test was conducted to determine the statistical significance of depth-wise and spatiotemporal variation in the b-value. The spatial distribution of the b-value estimated for each grid is presented in Table 4.9.

Table 4.9: The spatial distribution of b-value for each square grid is listed in the table.

Longitude (^{0})	Latitude (^{0})	b-value
80-82	26-28	-
80-82	28-30	0.66
80-82	30-32	0.75
82-84	26-28	1.24
82-84	28-30	0.77
82-84	30-32	0.92
84-86	26-28	0.93
84-86	28-30	0.93
84-86	30-32	0.76
86-88	26-28	0.68
86-88	28-30	0.92
86-88	30-32	0.69
88-90	26-28	0.71
88-90	28-30	0.91
88-90	30-32	0.67

4.5.5. Results and Discussions

4.5.5.1. Spatial Analysis of b-value

The geospatial distribution of b-value in Nepal and its surrounding area is depicted in Figure 4.47, revealing a range of b-values estimated using the Aki-Utsu MLE ([14], [15]). The b-value varies from 0.66 to 1.24 across the study area (Table 4.9), with corresponding SD spatially represented in Figure 4.48. Regions with insufficient seismic data yield undefined b-values, highlighted in grey. Notably, recent earthquakes, such as the one on November 9, 2022 (6.3), occurred in low b-value zones, suggesting potential future seismic activity. Statistical significance of b-value distribution was validated using the K-S non-parametric test. The parameters for the K-S test are detailed in Table 4.10, emphasizing the importance of statistical methods in analysing seismic data.

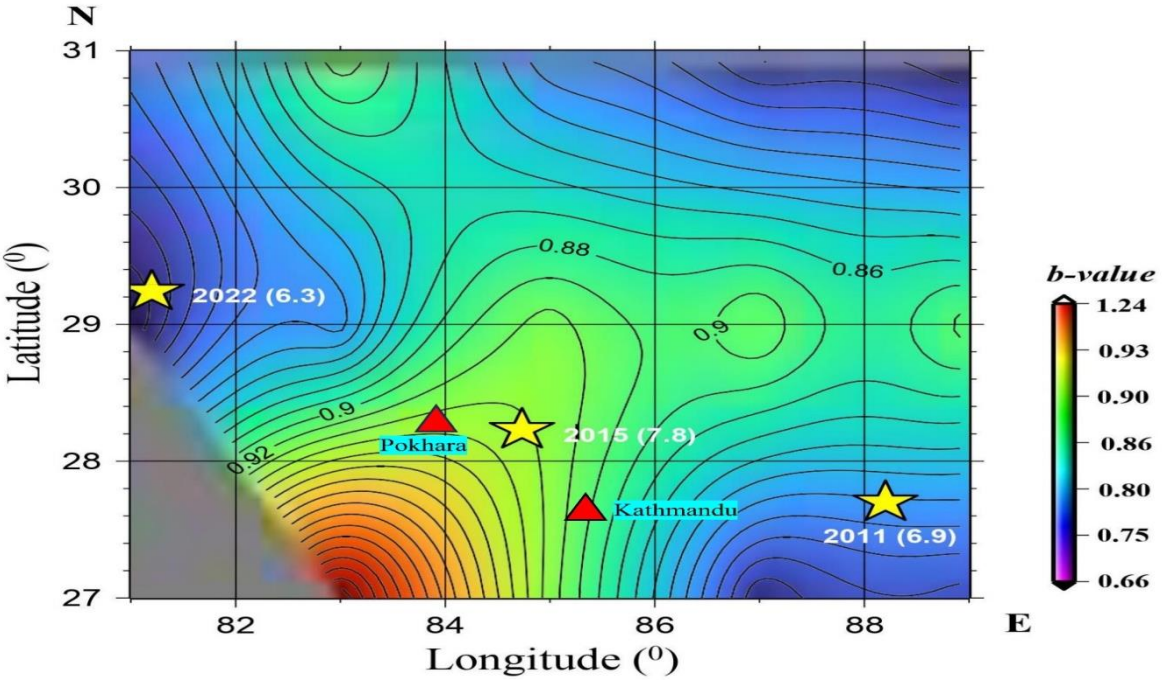

Figure 4.47: The geospatial distribution of the b-value for the study region. The epicentral location of 2011 (6.8), 2015 (7.8) and 2022(6.3) earthquakes observed in the studied region is shown by yellow stars.

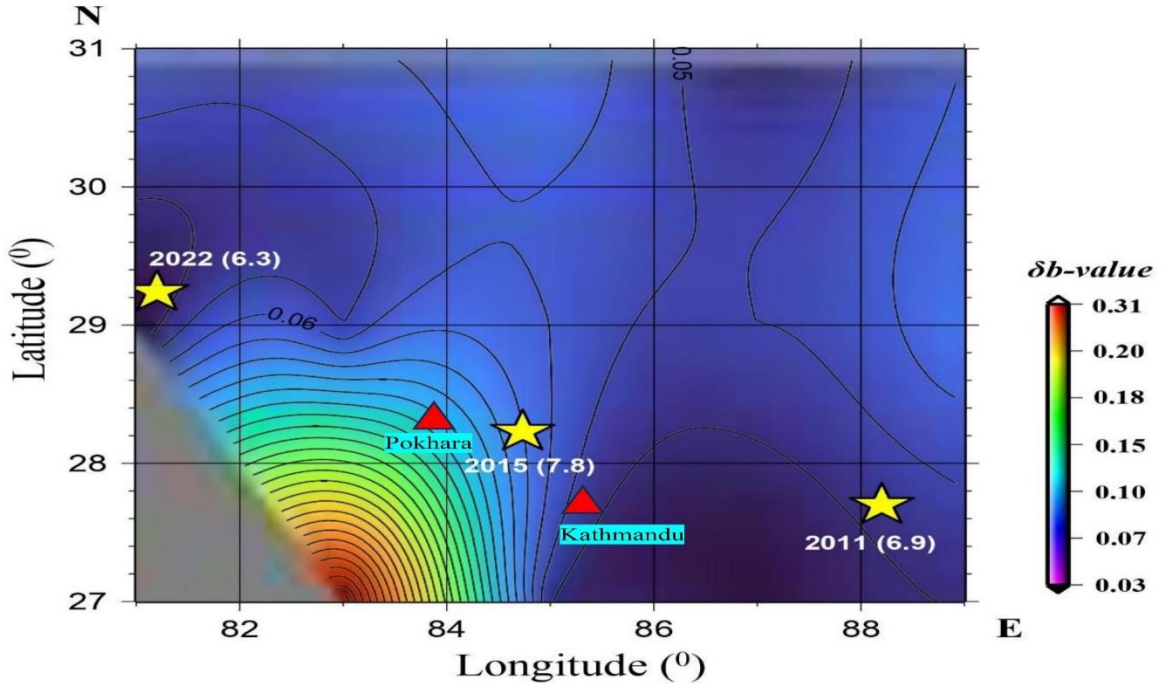

Figure 4.48: The geospatial distribution of standard deviation in b-value for the study region. Yellow star shows the epicentral location of 2011 (6.8), 2015 (7.8) and 2022 (6.3) earthquake.

Table 4.10: The parameters used for K-S test to testify the significance of geospatial distribution of b-value are listed in the table.

b-value	Freq	Cum Freq	ECDF	Z-value	SCDF	D-value
0.66	1	1	0.072	-1.022	0.154	0.083
0.67	1	2	0.143	-0.96	0.169	0.026
0.68	1	3	0.215	-0.898	0.185	0.03
0.69	1	4	0.286	-0.836	0.202	0.084
0.71	1	5	0.358	-0.711	0.239	0.119
0.75	1	6	0.429	-0.462	0.323	0.107
0.76	1	7	0.5	-0.4	0.345	0.156
0.77	1	8	0.572	-0.338	0.368	0.204
0.91	1	9	0.643	0.534	0.703	0.061
0.92	2	11	0.786	0.596	0.725	0.062
0.93	2	13	0.929	0.658	0.745	0.185
1.24	1	14	1	2.586	0.996	0.005

The K-S test evaluates the statistical significance of the geographical distribution of b-values. In Table 4.10, the parameters for the K-S test are outlined. With a sample size of 14 and significance levels set at p = 0.02 and p = 0.05, the maximum D-value (Dmax = 0.204) exceeds the critical D-value, indicating a substantial difference in b-value distribution across the region (Figure 4.49).

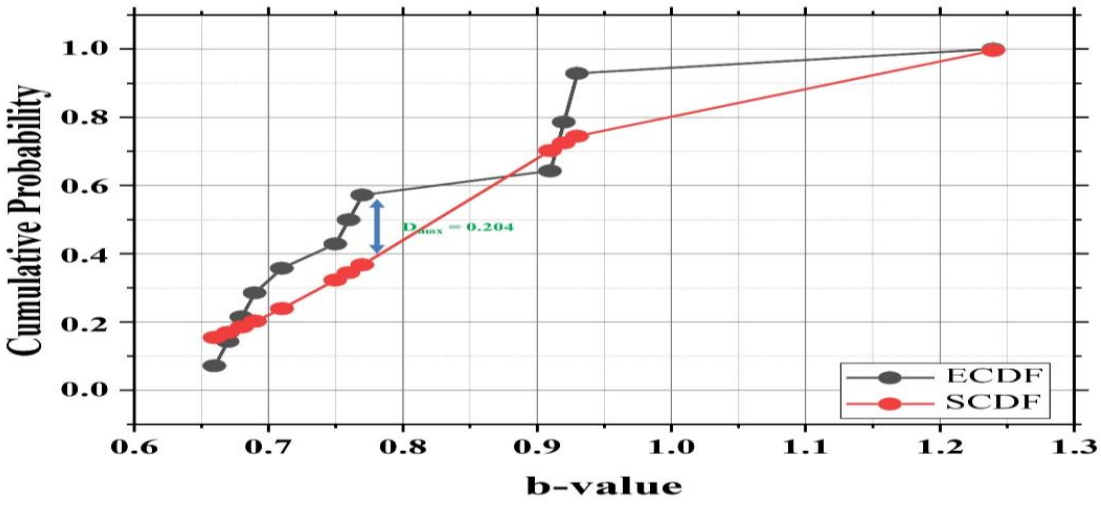

Figure 4.49: The Cumulative probability versus b-value to testify the significance of geospatial distribution of b-value.

4.5.5.2. Temporal analysis of b-value

Figure 4.50 illustrates the temporal evolution of the b-value in the examined area. Utilizing a window of fifty events with a shifting step of ten samples, the b-value exhibited a decreasing trend prior to the seismic event on November 9, 2022. Studies in Sumatra, southwest China, Hokkaido, Japan, and southern California also noted correlations between low b-values and impending earthquakes ([40], [66]). The negative gradient of the b-value slope preceding significant earthquakes suggests its potential as a precursor. The temporal fluctuation of the b-value curve in our analysis, showing a decrease before the November 9, 2022 earthquake, was validated using the non-parametric K-S test, indicating its statistical significance.

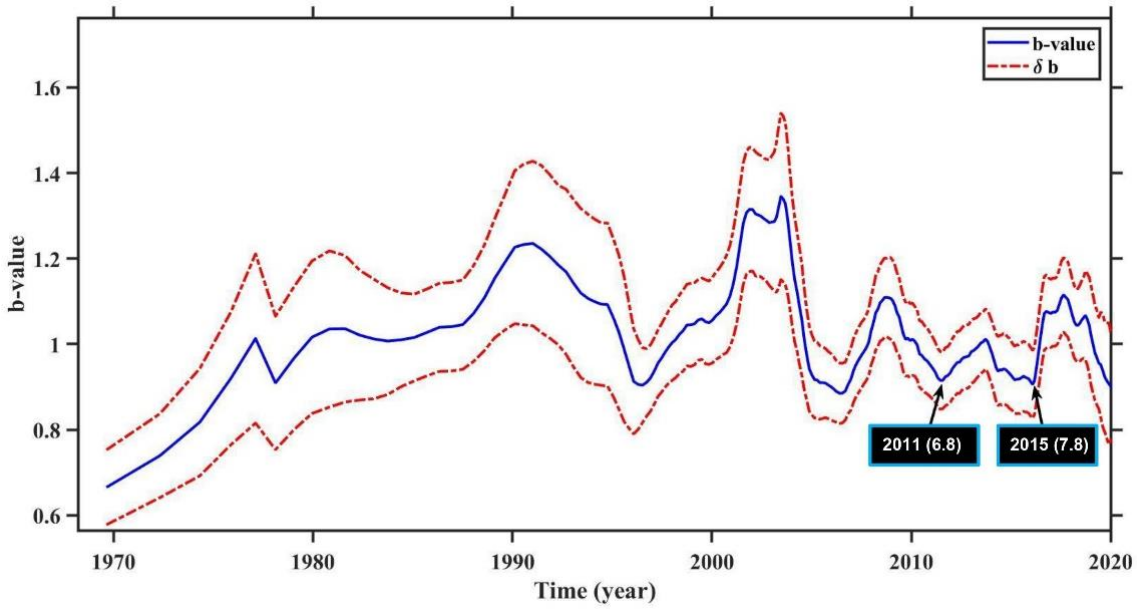

Figure 4.50: The temporal fluctuation curve of b-value for the study region. The fall in b-value before 2011 (6.8) and 2015 (7.8) is illustrated in the figure.

The relevance of temporal b-value variations demonstrated with the K-S test. Table 4.11 lists K-S test results. Figure 4.51 indicates Dmax exceeding critical values for significance, confirming b-value distribution differences.

Table 4.11: The parameters used to testify significance of temporal variation in b-value using K-S test.

b-value	Freq	Cum Freq	ECDF	Z-value	SCDF	D-value
0.916	1	1	0.112	-1.08	0.141	0.029
0.918	1	2	0.223	-0.834	0.203	0.02
0.919	2	4	0.445	-0.71	0.239	0.206
0.922	1	5	0.556	-0.34	0.368	0.189
0.925	1	6	0.667	0.031	0.513	0.155
0.927	1	7	0.778	0.278	0.61	0.169
0.93	1	8	0.889	0.648	0.742	0.148
0.941	1	9	1	2.006	0.978	0.023

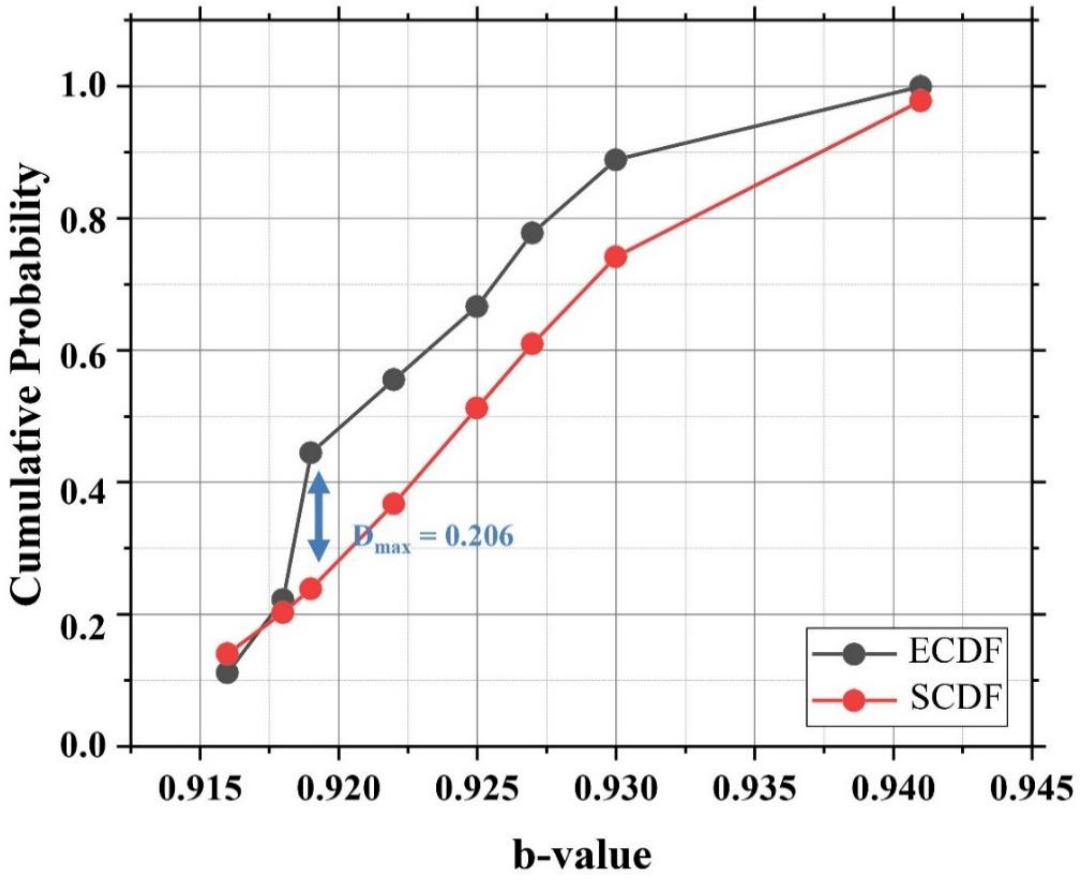

Figure 4.51: The Cumulative probability versus b-value to testify the significance of temporal distribution of b-value.

4.5.5.3. Depth-wise distribution of b-value

Several studies [75] have inferred that the b-value tends to change with the depth. Generally, the b-value tends to decrease with depth, meaning that smaller earthquakes are relatively more common at greater depths compared to larger ones [4]. This pattern can be attributed to various factors, such as changes in stress, rock properties, and the mechanics of faulting. At shallower depths, the brittle behavior of rocks may result in a higher proportion of larger earthquakes, leading to a higher b-value. Conversely, at greater depths, where rocks may deform ductilely and under higher pressures, smaller earthquakes become relatively more frequent, resulting in a lower b-value [3]. Understanding the variation of b-value with depth is crucial for seismic hazard assessment and earthquake forecasting. Figure 4.52 graphically illustrates the depth wise variation of the b-value for the study region. We determined the b-value for each window while keeping the M_C constant, utilizing a sample window of 50 events. The MLE [14] is applied for the approximation of the b-value for each window. Seismic occurrences predominantly fall within a depth range of up to 70 km, as depicted in Figures 4.44 and 4.53. Upon visually examining Figure 4.52, we observed a rapid increase in the b-value for depth ranges of 5 to 10 km and 30 to 40 km, followed by a gradual decrease in deeper regions (depth > 40km). The decrease in b-value in deeper regions is due to tectonic and geological factors, such as the transition from brittle to ductile deformation with increasing depth. Higher temperatures and pressures promote ductile deformation, resulting in fewer but larger-magnitude earthquakes. Deeper earthquakes in Nepal are often associated with the subduction of the Indian plate beneath the Eurasian plate. In a recent study, [4] identified a low b-value in the upper crust, indicating substantial stress accumulation in the Indo-Burma region of northeast India. In our current study, we observed lower b-values between 10 and 30 kms deep, while noting a sharp increase in b-values between 30 and 40 kms deep. This notable rise in b-values within this depth range can be attributed to the occurrence of larger magnitude earthquakes in the study region. Furthermore, we employed the non-parametric K-S test to assess the statistical significance of depth-wise b-value variation, deviating from the conventional method of visual analysis. We divided the 70 km depth region into subsections of 5 km depth each and recorded the corresponding b-value for each subsection to conduct the statistical significance test. Subsequently, the K-S test was performed on these recorded values. Detailed information about the variables used to validate the statistical significance of the b-value is provided in Table 4.12. For the K-S

test, a sample size of n = 12 was utilized, and the significance thresholds were set at 0.05 and 0.02, respectively. The maximum D-value (Dmax) was determined to be 0.118, as depicted in Table 4.12 and Figure 4.54. In our analysis, it was found that the observed maximum D-value exceeded the critical D-value at the significance levels of p = 0.05 and p = 0.02 with n = 12. This outcome of the K-S test confirms the fluctuation observed in depth-wise b-value variation, as the maximum D-value surpasses the critical D-value. The tectonic relevance of depth-wise b-value has been a subject of debate among academics worldwide due to its proven statistical significance using the non-parametric K-S test.

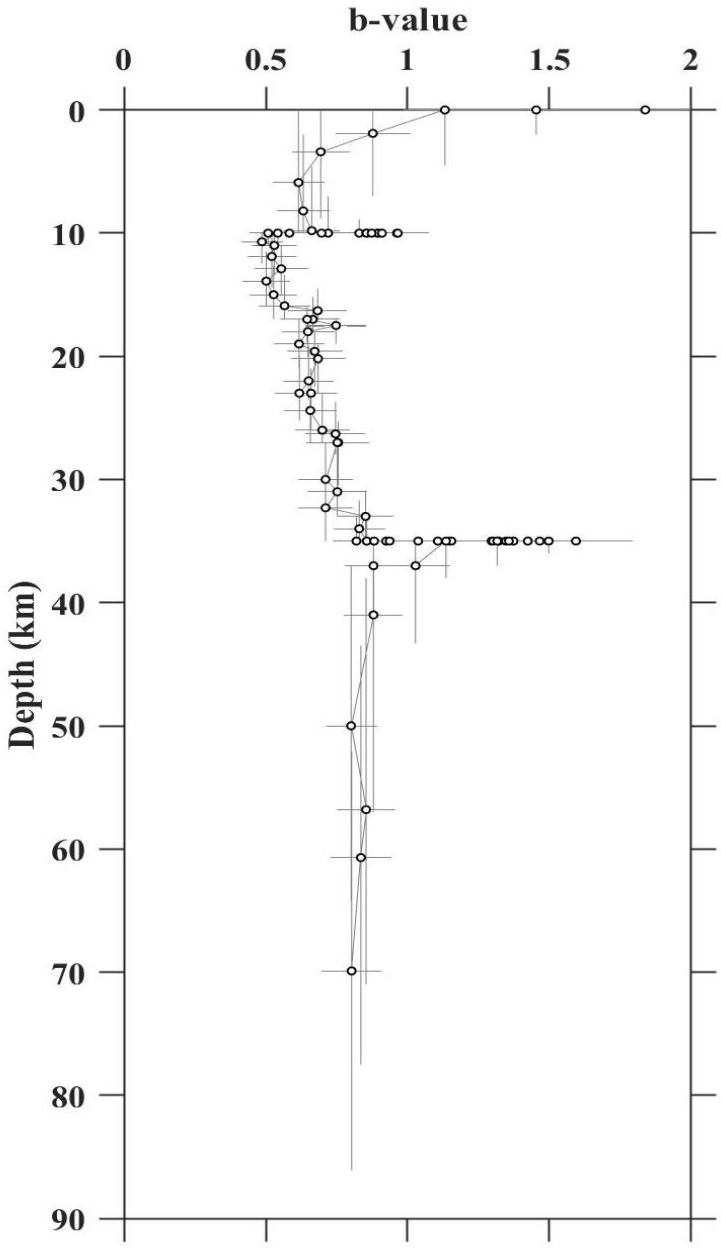

Figure 4.52: The depth wise distribution of b-value for the study region.

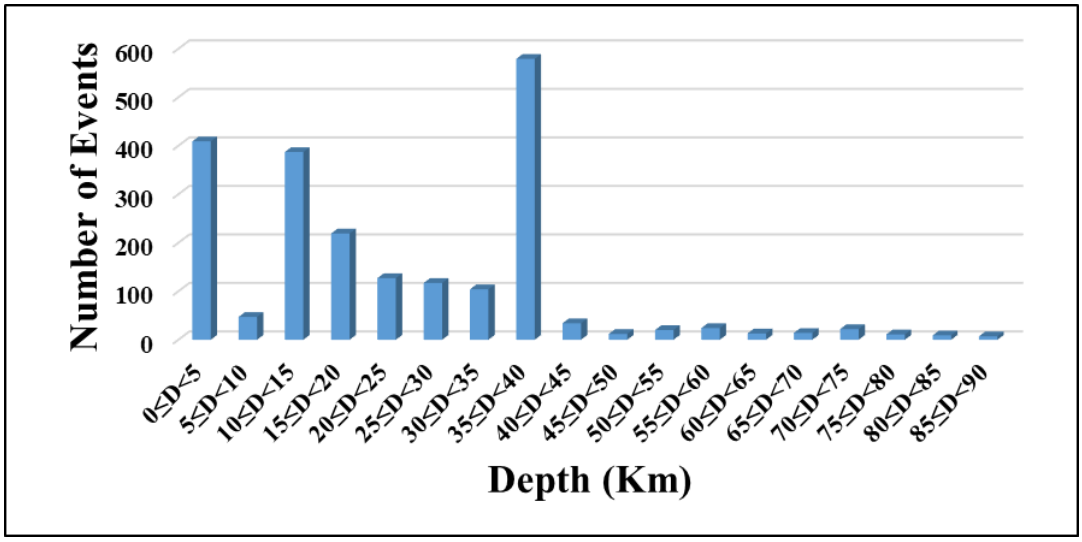

Figure 4.53: The Depth wise events distribution plot for the study region.

Table 4.12: Parameters of statistical significance of depth wise distribution of b-value using K-S test.

b-value	Freq	Cum Freq	ECDF	Z-value	SCDF	D-value
0.528	1	1	0.084	-1.955	0.026	0.059
0.615	1	2	0.167	-1.178	0.12	0.048
0.657	1	3	0.25	-0.803	0.212	0.039
0.684	1	4	0.334	-0.562	0.288	0.047
0.711	1	5	0.417	-0.321	0.375	0.043
0.72	1	6	0.5	-0.241	0.406	0.095
0.801	1	7	0.584	0.483	0.686	0.103
0.803	1	8	0.667	0.501	0.692	0.026
0.854	2	10	0.834	0.957	0.831	0.003
0.856	1	11	0.917	0.974	0.835	0.082
0.88	1	12	1	1.189	0.883	0.118

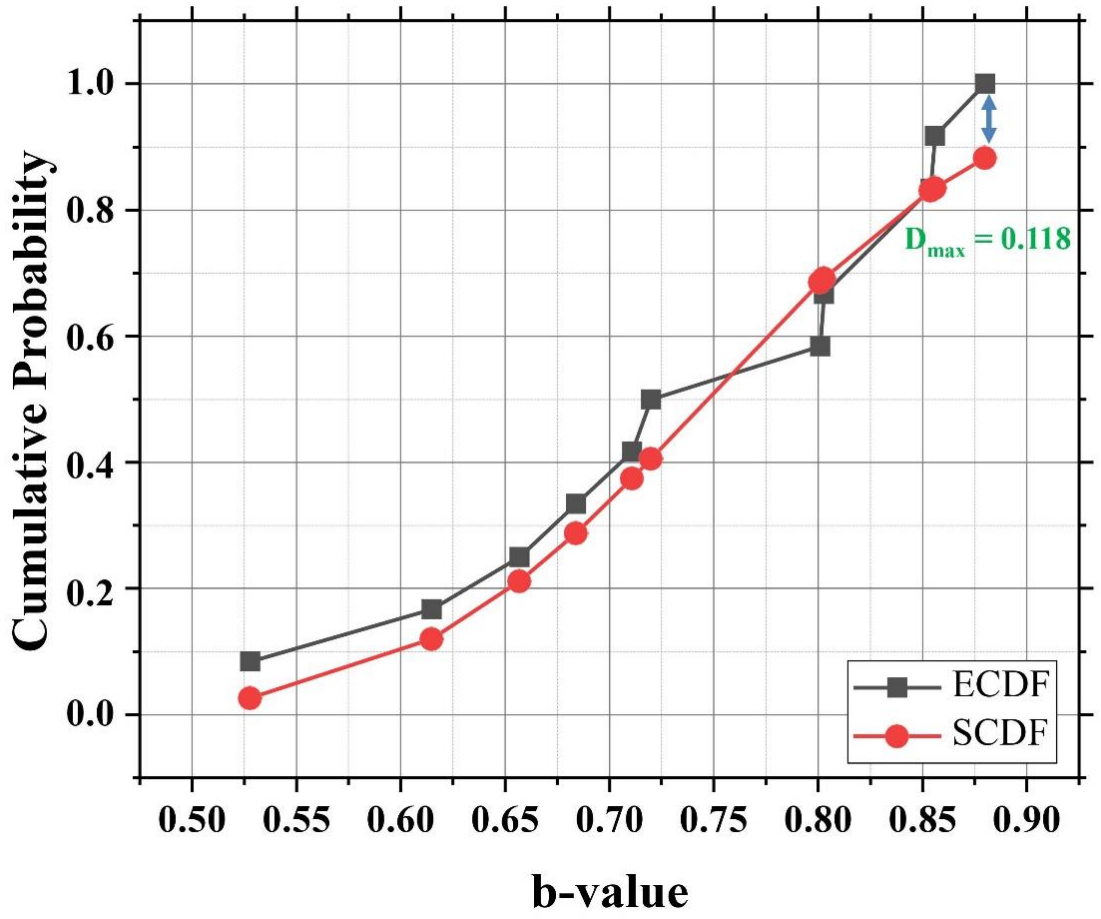

Figure 4.54: Cumulative probability versus b-value plot illustrating the statistical significance of depth-wise b-value distribution for the study region.

4.6. References

[1] England, P. and Bilham, R. The Shillong Plateau and the Great 1897 Assam Earthquake. *Tectonics,* 34(9): 1792-1812, 2015.

[2] Gutenberg, B. and Richter, C. F. Frequency of Earthquakes in California. *Bulletin of the Seismological Society of America,* 34(4): 185-188, 1944.

[3] Khan, P. K. and Chakraborty, P. P. The seismic b-value and its correlation with Bouguer gravity anomaly over the Shillong Plateau area: Tectonic implications. *Journal of Asian Earth Sciences,* 29(1): 136–147, 2007.

[4] Bora, D. K., Borah, K., Mahanta, R. and Borgohain, J. M. Seismic b-Values and Its Correlation with Seismic Moment and Bouguer Gravity Anomaly over Indo-Burma Ranges of Northeast India: Tectonic Implications. *Tectonophysics,* 728-729: 130-141, 2018.

[5] Kamer, Y. and Hiemer, S. Data-Driven Spatial b Value Estimation with Applications to California Seismicity: To b or Not to b. *Journal of Geophysical Research: Solid Earth,* 120(7): 5191-5214, 2015.

[6] Schorlemmer, D., Wiemer, S. and Wyss, M. Variations in Earthquake-Size Distribution Across Different Stress Regimes. *Nature,* 437(7058): 539-542, 2005.

[7] Nanjo, K. Z., Hirata, N., Obara, K. and Kasahara, K. Decade-scale decrease in b value prior to the M9-class 2011 Tohoku and 2004 Sumatra quakes. *Geophysical Research Letters,* 39: L20304, 2012.

[8] Borgohain, J. M., Borah, K., Biswas, R. and Bora, D. K. Seismic b-value anomalies prior to the 3rd January 2016, Mw = 6.7 Manipur earthquake of northeast India. *Journal of Asian Earth Sciences, 154*: 42–48, 2018.

[9] Roy, A. B. and Purohit, R. The Himalayas: Evolution Through Collision. In *Introduction to the Himalaya* (eds. Roy, A. B. & Purohit, R.) 311-327 (Elsevier, 2018).

[10] Sharma, S., Sarma, J. and Baruah, S. Dynamics of Mikir Hills Plateau and Its Vicinity: Inferences on Kopili and Bomdila Faults in Northeastern India Through Seismotectonics, Gravity and Magnetic Anomalies. *Annals of Geophysics,* 61(3): (2018).

[11] Reasenberg, P. Second-Order Moment of Central California Seismicity, 1969-1982. *Journal of Geophysical Research,* 90(B7): 5479-5495, 1985.

[12] Nath, S. K., Mandal, S., Adhikari, M. D. and Maiti, S. K. A Unified Earthquake Catalogue for South Asia Covering the Period 1900-2014. *Natural Hazards,* 85(3): 1787-1810, 2017.

[13] Bora, D. K. Scaling Relations of Moment Magnitude, Local Magnitude, and Duration Magnitude for Earthquakes Originated in Northeast India. *Earthquake Science,* 29(3): 153-164, 2016.

[14] Aki, K. Maximum likelihood estimate of b in the formula log N= a-bm and its confidence limits. *Bulletin of Earthquake Research Institute Tokyo University,* 43: 237–239, 1965.

[15] Utsu, T. A Method for Determining the Value of the Formula logN=a-bM Showing the Magnitude-Frequency Relation for Earthquakes. *Geophysical bulletin of Hokkaido University,* 13: 99–103, 1965.

[16] Shi, Y. and Bolt, B. A. The Standard Error of the Magnitude-Frequency b Value. *Bulletin of the Seismological Society of America,* 72(5): 1677-1687, 1982.

[17] Kamer, Y. Comment on “Systematic survey of high-resolution b value imaging along Californian faults: Inference on asperities” by T. Tormann et al. *Journal of Geophysical Research: Solid Earth,* 119(7): 5830–5833, 2014.

[18] Kamer, Y. and Hiemer, S. Comment on "Analysis of the b-Values Before and After the 23 October 2011 Mw 7.2 Van-Erciş, Turkey, Earthquake." *Tectonophysics,* 608: 1448-1451, 2013.

[19] Mousavi, S. M. Spatial variation in the frequency-magnitude distribution of earthquakes under the tectonic framework in the Middle East. *Journal of Asian Earth Sciences, 147*: 193–209, 2017.

[20] Schorlemmer, D., Wiemer, S. and Wyss, M. Earthquake statistics at Parkfield: 1. Stationarity of b values. *Journal of Geophysical Research: Solid Earth,* 109(B12): 2004.

[21] Wiemer, S. A software package to analyze seismicity: Zmap. *Seismological Research Letters,* 72(3): 373–382, 2001.

[22] Bhattacharya, P., Majumdar, R. K. and Kayal, J. Fractal dimension and b-value mapping in Northeast India. *Current Science,* 82: 1486–1491, 2002.

[23] Khan, P. K., Ghosh, M., Chakraborty, P. P. and Mukherjee, D. Seismic b-value and the assessment of ambient stress in Northeast India. *Pure and Applied Geophysics,* 168(10): 1693–1706, 2011.

[24] Tormann, T., Enescu, B., Woessner, J. and Wiemer, S. Randomness of megathrust earthquakes implied by rapid stress recovery after the Japan earthquake. *Nature Geoscience,* 8(2):152–158, 2015.

[25] Sharma, S. and Baruah, S. Modelling of the Kopili Fault based on slip rate, moment rate and seismic activity in Mikir Hills Plateau of Northeastern India. *Geomatics, Natural Hazards and Risk,* 8(2): 1157–1172, 2017.

[26] Biswas, R. A brief review of the recent Assam earthquake. *5*, 1–2 (2021).

[27] Hurukawa, N., Tun, P. P. and Shibazaki, B. Detailed geometry of the subducting India Plate beneath the Burma Plate and subcrustal seismicity in the Burma Plate derived from joint hypocenter relocation. *Earth, Planets and Space,* 64(4): 333–343, 2012.

[28] Monterroso, D. A. and Kulhánek, O. Spatial variations of b-values in the subduction zone of Central America. *Geofisica Internacional,* 42(4): 575–587, 2003.

[29] Wiemer, S. and Benoit, J. P. Mapping the b-value anomaly at 100 km depth in the Alaska and New Zealand subduction zones. *Geophysical Research Letters,* 23(13): 1557–1560, 1996.

[30] Ruff, L. and Kanamori, H. Seismicity and the subduction process. *Physics of the Earth and Planetary Interiors,* 23(3): 240–252, 1980.

[31] Bureau of Indian Standard. Indian standard, criteria for earthquake resistance design of structures, fifth revision, part-I. New Delhi, India: Author (2002).

[32] Hurukawa, N. and Maung, P. M. Two seismic gaps on the Sagaing Fault, Myanmar, derived from relocation of historical earthquakes since 1918. *Geophysical Research Letters,* 38 (L01310): 2011.

[33] Gahalaut, V. K. and Kundu, B. The January 4, 2016 Manipur earthquake in the Indo-Burmese wedge, an intra-slab event. *Geomatics, Natural Hazards and Risk,* 7(5): 1506–1512, 2016.

[34] Wiemer, S. and Wyss, M. Minimum magnitude of completeness in earthquake catalogs: examples from Alaska, the Western United States, and Japan. *Bulletin of the Seismological Society of America,* 90(4): 859–869, 2000.

[35] Woessner, J. and Wiemer, S. Assessing the quality of earthquake catalogues: estimating the magnitude of completeness and its uncertainty. *Bulletin of the Seismological Society of America,* 95(2), 684–698 (2005).

[36] Schorlemmer, D., Neri, G., Wiemer, S. and Mostaccio, A. Stability and significance tests for b-value anomalies: example from the Tyrrhenian Sea. *Geophysical Research Letters,* 30(16):1835, 2003.

[37] Xie, Z., Lyu, Y. and Li, X. Temporal and spatial changes in the b-value prior to the 2021 Luxian MS 6.0 earthquake in Sichuan, China. *Geomatics, Natural Hazards and Risk,* 13(1), 934–948, 2022.

[38] Bora, D. K., Borah, K., Singh, A. P. and Mishra, O. P. Distribution of b-values in Indo-Burma Ranges, northeast India: implications to structural heterogeneities and style of faulting. *Geological Journal, 57:* 5284-5293, 2021.

[39] Kundu, B. and Gahalaut, V. K. Earthquake occurrence processes in the Indo-Burmese wedge and Sagaing fault region. *Tectonophysics,* 524–525: 135–146, 2012.

[40] Nuannin, P., Kulhanek, O. and Persson, L. Spatial and temporal b value anomalies preceding the devastating off coast of NW Sumatra earthquake of December 26, 2004. *Geophysical Research Letters,* 32 (L11309): 2005.

[41] Kundu, B. and Gahalaut, V. K. Tectonic geodesy revealing geodynamic complexity of Indo-Burmese arc region, North East India. *Current Science,* **104**: 920–933, 2013.

[42] Ashtari Jafari, M. The distribution of b-value in different seismic provinces of Iran. *Journal of Geodynamics,* 103: 26–41, 2008.

[43] Hazarika, D. and Kayal, J. R. Recent felt earthquakes (Mw 5.0–5.9) in Mizoram of north-east India region: seismotectonics and precursor appraisal. *Geological Journal,* 57(2): 877–885, 2022.

[44] Xie, W., Hattori, K. & Han, P. Temporal variation and statistical assessment of the b value off the pacific coast of Tokachi, Hokkaido, Japan. *Entropy, 21(3):* 249, 2019.

[45] Rehman, K. et al. Spatio-temporal variations of b-value in and around north Pakistan. *Journal of Earth System Science,* 124(7): 1445–1456, 2015.

[46] Sanchez, J. J. Spatial variations in the frequency–magnitude distribution of earthquakes at Mount Pinatubo volcano. *Bulletin of the Seismological Society of America,* 94(2): 430–438, 2004.

[47] Maden, N. and Öztürk, S. Seismic b-values, Bouguer gravity and heat flow data beneath eastern Anatolia, Turkey: tectonic implications. *Surveys in Geophysics, 36(4):* 549–570, 2015.

[48] Mousavi, S. M. Mapping seismic moment and b-value within the continental-collision orogenic-belt region of the Iranian Plateau. *Journal of Geodynamics, 103:* 26–41, 2017.

[49] Monterroso, D. A. and Kulhánek, O. Spatial variations of b-values in the subduction zone of Central America. *Geofísica Internacional, 42(4)*: 575–587, 2003.

[50] Karabulut, H., Güvercin, S. E., Hollingsworth, J. & Konca, A. Ö. Long silence on the East Anatolian Fault Zone (Southern Turkey) ends with devastating double earthquakes (6 February 2023) over a seismic gap: implications for the seismic potential in the Eastern Mediterranean region. *Journal of the Geological Society,* 180(3): 2023.

[51] Duman, T. Y.; Çan, T.; Emre, Ö.; Kadirioğlu, F. T.; Başarır Baştürk, N.; Kılıç, T.; Arslan, S.; Özalp, S.; Kartal, R. F.; Kalafat, D.; Karakaya, F.; Eroğlu Azak, T.; Özel, N. M.; Ergintav, S.; Akkar, S.; Altınok, Y.; Tekin, S.; Cingöz, A.; Kurt, A. İ. Seismotectonic Database of Turkey. *Bulletin of Earthquake Engineering,* 16(8): 3277–3316, 2018.

[52] Tan, O. A Homogeneous Earthquake Catalogue for Turkey. *Natural Hazards and Earth System Sciences***,** 21(7): 2059–2073, 2021.

[53] Uhrhammer, R. A. Characteristics of Northern and Central California Seismicity. *Earthquake Notes*, 57(1): 21, 1986.

[54] Stepp, J. Analysis of Completeness of the Earthquake Sample in the Puget Sound Area and Its Effect on Statistical Estimates of earthquake Hazard. *Proceedings of the 1st International Conference Microzonazion* Seattle 2: 897–910, 1972.

[55] Tinti, S. and Mulargia, F. Effects of Magnitude Uncertainties in the Gutenberg-Richter Frequency-Magnitude Law. *Bulletin of the Seismological Society of America*, 75: 1681-1697, 1985.

[56] Alkan, H., Öztürk, S. and Akkaya, İ. Seismic Hazard Implications in and Around the Yedisu Seismic Gap (Eastern Türkiye) Based on Coulomb Stress Changes, b-Values, and S-Wave Velocity. *Pure and Applied Geophysics*, 180: 3227–3248, 2023.

[57] Utkucu, M., Kurnaz, T. F. and İnce, Y. The Seismicity Assessment and Probabilistic Seismic Hazard Analysis of the Plateau Containing Large Dams Around the East Anatolian Fault Zone, Eastern Türkiye. *Environmental Earth Sciences,* 82(15): 371, 2023.

[58] Öztürk, S. Earthquake Hazard Potential in the Eastern Anatolian Region of Turkey: Seismotectonic b and Dc-Values and Precursory Quiescence Z-Value. *Frontiers in Earth Science,* 12(1): 215–236, 2018.

[59] Scholz, C. H. The Frequency-Magnitude Relation of Micro-fracturing in Rock and Its Relation to Earthquakes. *Bulletin of the Seismological Society of America,* 58 (1): 399–415, 1968.

[60] Öztürk, S. Space-Time Assessing of the Earthquake Potential in Recent Years in the Eastern Anatolia Region of Turkey. *Earth Sciences Research Journal,* 21(2): 67–75, 2017.

[61] Westerhaus, M. et al. Correlating Variations of b Values and Crustal Deformations During the 1990s May Have Pinpointed the Rupture Initiation of the Mw = 7.4 Izmit Earthquake of 1999 August 17. *Geophysical Journal International,* 148: 139–152, 2002.

[62] Görgün, E. Analysis of the b-Values Before and After the 23 October 2011 MW 7.2 Van–Erciş, Turkey Earthquake. *Tectonophysics,* 603: 213–221, 2013.

[63] Chen, X., Li, Y. and Chen, L. The Characteristics of the b-Value Anomalies Preceding the 2004 Mw9.0 Sumatra Earthquake. *Geomatics, Natural Hazards and Risk,* 13(1): 390–399, 2022.

[64] Katsumata, K. Imaging the High b-Value Anomalies Within the Subducting Pacific Plate in the Hokkaido Corner. *Earth Planets Space*, 58 (11): e49–e52, 2006.

[65] Polat, G. Spatial Analysis of b-Value Variability in Elazig City and the Surrounding Area (Eastern Turkey). *Acta Geophysica,* 70(1): 15–25, 2022.

[66] Zhang, S. and Zhou, S. Spatial and Temporal Variation of B-Values in Southwest China. *Pure and Applied Geophysics,* 173(1): 85–96, 2016.

[67] Henderson, J. R., Main, I. G., Pearce, R. G. and Takeya, M. K. Seismicity in North-Eastern Brazil – Fractal Clustering and the Evolution of the b-Value. *Geophysical Journal International,* 116(1): 217–226, 1994.

[68] Chen, J. and Zhu, S. Spatial and Temporal b-Value Precursors Preceding the 2008 Wenchuan, China, Earthquake (Mw = 7.9): Implications for Earthquake Prediction. *Geomatics, Natural Hazards and Risk,* 11(1): 1196–1211, 2020.

[69] Bayrak, E. and Ozer, C. The 24 January 2020 (Mw 6.8) Sivrice (Elazig, Turkey) Earthquake: A First Look at Spatiotemporal Distribution and Triggering of Aftershocks. *Arabian Journal of Geosciences,* 14 (22): 2445, 2021.

[70] Stevens, V. L., Shrestha, S. N. and Maharjan, D. K. Probabilistic seismic hazard assessment of Nepal. *Bulletin of the Seismological Society of America,* 108(6): 3488–3510, 2018.

[71] Tiwari, R. K., Paudyal, H. and Shanker, D. On the Spatio-temporal Variation in b-Value After 25 April 2015 Gorkha, Nepal Earthquake. *Geodesy and Geodynamics,* 13 (5): 525–533, 2022.

[72] Parajuli, H. R., Bhusal, B. and Paudel, S. Seismic zonation of Nepal using probabilistic seismic hazard analysis. *Arabian Journal of Geosciences,* 14(20): 2021.

[73] Copley, A., Avouac, J. P. and Royer, J. Y. India-Asia collision and the Cenozoic slowdown of the Indian plate: Implications for the forces driving plate motions. *Journal of Geophysical Research: Solid Earth,* 115(B3): 2010.

[74] Kolathayar, S., Sitharam, T. G. and Vipin, K. S. Spatial variation of seismicity parameters across India and adjoining areas. *Natural Hazards,* 60(3): 1365–1379, 2012.

[75] Rahman, Z. and Rehman, K. Seismic b value analysis of north Pakistan: an appraisal. *Environmental Earth Sciences*, 83(1): 2, 2024.